

Correspondence to: Prof Paul J. Low
Department of Chemistry
Durham University
South Rd, Durham, DH1 3LE, UK
p.j.low@durham.ac.uk

**Synthesis, structure and redox properties of tris(pyrazolyl)borate-capped
ruthenium vinyl complexes.[†]**

Julian D. Farmer,^a Wing Y. Man,^a Mark A. Fox,^a Dmitry S. Yufit,^a Judith A.K. Howard,^a Anthony F. Hill,^b Paul J. Low.^{a*}

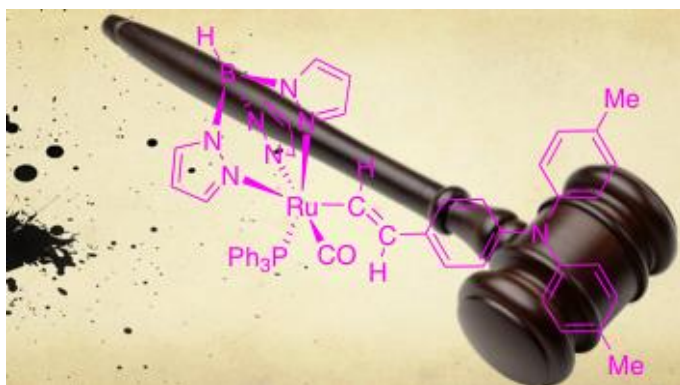
^a *Department of Chemistry, Durham University, South Rd, Durham, DH1 3LE, UK*

^b *Research School of Chemistry, Australian National University, Canberra, ACT, 0200, Australia.*

[†] Dedicated to Professor Thomas P. Fehlner, in recognition of his outstanding contributions to organometallic chemistry.

Abstract

Reaction of RuHCl(CO)(PPh₃)₃ with aryl alkynes HC≡CC₆H₄R'-4 [**1**: R' = N(C₆H₄Me-4)₂ (**a**), OMe (**b**), Me (**c**), CO₂Me (**d**), NO₂ (**e**)] gives the five-coordinate vinyl complexes Ru(CH=CHC₆H₄R'-4)Cl(CO)(PPh₃)₂ (**2a - e**). Reaction of **2a** with excess PMe₃ gives crystallographically characterised Ru{CH=CHC₆H₄N(C₆H₄Me-4)₂-4}Cl(CO)(PMe₃)₃ (**3a**), whilst reaction of **2a - e** with KTp affords Ru(CH=CHC₆H₄R'-4)(CO)(PPh₃)Tp (**4a-e**) bearing the *facially* capping Tp⁻ ligand. Electrochemical and spectroelectrochemical properties of **4a - e** are consistent with substantial redox activity associated with the vinyl ligand, and these properties have been satisfactorily modelled by DFT based calculations of electronic structure.



Keywords Ruthenium; vinyl; redox non-innocence; spectroelectrochemistry

Highlights

- A series of ruthenium vinyl ligands featuring a facially capping tris(pyrazolyl)borate ligand have been prepared and structurally characterised.
- Electrochemical and spectroelectrochemical properties are consistent with substantial redox activity associated with the vinyl ligand
- DFT and TD DFT calculations are used in support of the spectroscopic information to give a detailed description of the electronic structure of these complexes.

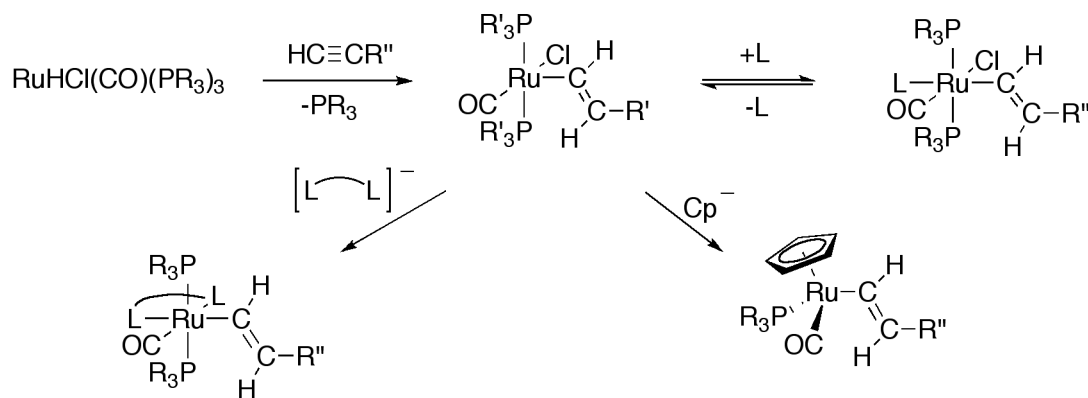
1. Introduction

The redox chemistry of Werner-style transition metal coordination complexes, $[ML_n]$, is usually governed by changes in the formal metal oxidation state and occupation of frontier orbitals with considerable metal d-orbital character. However, systems in which redox character is more closely associated with changes in population of ligand-based orbitals have long been recognised, and activity in the area has expanded from simple $O_2 / O_2^{\bullet-} / O_2^{2-}$ and $NO^+ / NO^{\bullet} / NO^-$ series through redox related families based on dithiolenes, diimines, *ortho*-quinones to an expansive range of larger heterocyclic and macrocyclic ligands. The combination of redox active metals with redox active ligands leads to considerable scope for ambiguity in oxidation state assignments [1], giving rise to descriptions of ‘innocent’ (those that allow unambiguous assignment of metal oxidation state) and ‘suspect’ ligands coined by Jorgensen [2]. In more recent times, the description of ligands as ‘suspect’, has often given way to descriptions in terms of ‘non-innocent’ behaviour, although this term should be reserved for systems in which the ligand has established redox activity, rather than the suspect character noted in Jorgensen’s review. It is also implicit in these descriptions that the behaviour of the ligand is strongly influenced by the nature of the metal fragment (metal and supporting ligands) to which it is coordinated, and the same ligand may display redox innocent or non-innocent behaviour depending on the relative redox potentials of the ligand and the supporting metal fragment, other potentially redox active ligands and the synergistic σ - and π -forward and back-bonding interactions [3-5]. Keeping the judicial parlance, spectroscopic evidence is required to establish the redox guilt or innocence of a ligand, often supported by quantum mechanical calculations [6]. Nevertheless, the capacity for both ligand and

metal to adjust redox state has considerable implications for the design of catalytic systems, with ligands used as electron reservoirs or sinks to help shuttle electrons to a substrate [7-9].

Within the span of complexes in which redox activity can be well described in terms of changes in metal (e.g. $[\text{Co}(\text{NH}_3)_6]^{2+/3+}$) [10] or ligand (e.g. $[\text{Cr}(\text{tBu}_2\text{-bpy})_3]^{3+/2+/1+/0}$) [11] oxidation state lie complexes of intermediate character in which the redox active orbitals have extensively mixed metal and ligand character. For this latter group there exists considerable ambiguity in terms of the precise oxidation states of either component [4]. However, the extensive mixing of metal-ligand character which complicates the assignment of accurate integer oxidation states to a particular atomic center in a strongly delocalised molecular framework underpins many of the fascinating optoelectronic properties of this class of metal complex [12]. It has now been firmly established that ruthenium alkynyl complexes $\text{Ru}(\text{C}\equiv\text{CR})(\text{PP})\text{Cp}'$ (P = phosphine, PP = bis(phosphine); $\text{Cp}' = \text{Cp}, \text{Cp}^*$) [13-15] and $\text{Ru}(\text{X})(\text{C}\equiv\text{CR}')(\text{PP})_2$ ($\text{X} = \text{Cl}, \text{C}\equiv\text{CR}'$) [16] feature such extensive mixing of the metal d and alkynyl ligand π -orbitals. Vinyl complexes $\text{Ru}(\text{CH}=\text{CHR}')(\text{Cl})(\text{CO})(\text{PR}_3)_2\text{L}$ ($\text{R}' = \text{Me}, \text{}^i\text{Pr}, \text{Ph}$; L = vacant coordination site, PR_3 , pyridine donor ligand, CO , NCR , etc) [17] also fall either in this latter 'delocalised' category for $\text{R}' = \text{H}, \text{Bu}^t, \text{Ph}$, and exhibit increasing degrees of ligand redox character as the alkynyl or vinyl ligand substituent R' is made progressively lower and lower in energy (e.g. 1-naphthyl, 9-anthryl, ethynylphenyl) [18-20], and when incorporated into bridging ligands spanning two strongly electron-donating ruthenium fragments [21-28].

The complexes $\text{Ru}(\text{CH}=\text{CHR}')(\text{Cl})(\text{CO})(\text{PR}_3)_2\text{L}$, which are readily prepared by insertion of an alkyne into the Ru–H bond in $\text{RuHCl}(\text{CO})(\text{PR}_3)_n$ ($n = 2, 3$) [29] offer an entry point to a wide range of vinyl complexes through facile substitution reactions of the supporting phosphine and chloride ligands by a wide range of neutral and anionic mono and bidentate ligands (Scheme 1) [30, 31]. The binding of the ligand trans to the vinyl ligand is weakened by the strong *trans* influence of the vinyl ligand, and in the case of bulky triaryl phosphines, PR_3 , the complexes are often isolated as the five-coordinate species ($\text{L} = \text{vacant site}$) [32-35], or exist as a mixture of the five- and six-coordinate complexes (Scheme 1) [36]. The five-coordinate species are convenient precursors to a range of derivatives through ligand substitution reactions [37- 44], giving considerable scope to tune the metal-ligand coordination sphere.



Scheme 1. A representative array of ligand substitution reactions associated with five-coordinate vinyl complexes $\text{Ru}(\text{CH}=\text{CHR}')(\text{Cl})(\text{CO})(\text{PR}_3)_2$.

This considerable flexibility in the coordination sphere presents a wide range of interesting possibilities for fine-tuning the degree of metal vs vinyl ligand redox character [5]; however, to date the vast majority of investigations of the redox chemistry of ruthenium vinyl complexes have been restricted to five-coordinate $\text{Ru}(\text{CH}=\text{CHR}')(\text{Cl})(\text{CO})(\text{P}^i\text{Pr}_3)_2$ systems [17, 18, 21-23, 45] or six-coordinate complexes $\text{Ru}(\text{CH}=\text{CHR})(\text{Cl})(\text{CO})(\text{PPh}_3)_2\text{L}$ (L = 4-ethyl-isonicotinate) [18], $\text{Ru}(\text{CH}=\text{CHR}')(\text{CO})(\text{O}_2\text{CR})(\text{P}^i\text{Pr}_3)_2$ [18] and $\text{Ru}(\text{CH}=\text{CHR})(\text{Cl})(\text{CO})(\text{PMe}_3)_3$ [28, 46].

In this report, we describe efforts to further tune the electronic character of the $\text{Ru}-\text{CH}=\text{CHR}''$ fragment through the preparation and study of the tris(pyrazolyl)borate (Tp^-) derivatives $\text{Ru}(\text{CH}=\text{CHC}_6\text{H}_4\text{R-4})(\text{CO})(\text{PPh}_3)\text{Tp}$. The tridentate tris(pyrazolyl)borate ligand occupies a facially capping position on the octahedral (six-coordinate) metal center [43], whilst the retention of the CO ligand provides a convenient $\nu(\text{CO})$ spectroscopic probe through which to assess the electron density at the metal center [17]. The details of the syntheses, structures and electrochemical properties of the complexes $\text{Ru}(\text{CH}=\text{CHC}_6\text{H}_4\text{R-4})(\text{CO})(\text{PPh}_3)\text{Tp}$ (R = $\text{N}(\text{C}_6\text{H}_4\text{Me-4})_2$, OMe, Me, CO_2Me , NO_2) are reported together with UV-vis-NIR and IR spectroelectrochemical studies of $[\text{Ru}(\text{CH}=\text{CHC}_6\text{H}_4\text{R-4})(\text{CO})(\text{PPh}_3)\text{Tp}]^{n+}$ (n = 0, 1). The resulting descriptions of the redox character of the vinyl ligand are supported by DFT calculations.

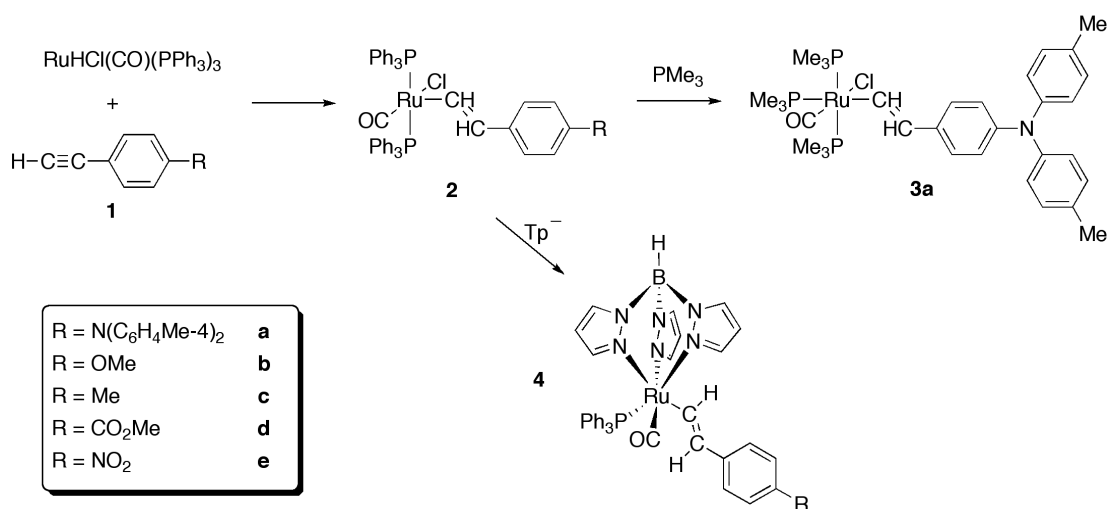
2. Results and Discussion

2.1 Syntheses

The reaction of terminal aryl alkynes, $\text{HC}\equiv\text{CC}_6\text{H}_4\text{R}-4$ [**1**: $\text{R} = \text{N}(\text{C}_6\text{H}_4\text{Me}-4)_2$ (**a**), OMe (**b**), Me (**c**), CO_2Me (**d**), NO_2 (**e**)], with $\text{RuHCl}(\text{CO})(\text{PPh}_3)_3$ in CH_2Cl_2 proceeded smoothly to give the five-coordinate complexes $\text{Ru}(\text{CH}=\text{CHC}_6\text{H}_4\text{R}-4)\text{Cl}(\text{CO})(\text{PPh}_3)_2$ (**2a - e**), evidenced by the developing red colouration of the reaction mixture (Scheme 2). Complex **2a** was isolated as a red solid, following a series of precipitations, and characterised by way of example. The IR spectrum of **2a** in CH_2Cl_2 solution was characterised by a strong $\nu(\text{CO})$ band at 1932 cm^{-1} , which compares with other five-coordinate species $\text{Ru}(\text{CH}=\text{CHPh})\text{Cl}(\text{CO})(\text{PR}'_3)_2$ ($\text{R}' = \text{Ph}$, 1927 cm^{-1} ; $i\text{Pr}$, 1911 cm^{-1}) and reflects the relative sensitivity of the $\nu(\text{CO})$ frequency to the electron-donating character of the P^iPr_3 and PPh_3 ligands, and relative insensitivity to the nature of the vinyl ligand substituent [18]. In addition, the vinyl protons were identified from coupled resonances at 5.54 (d, $J_{\text{HH}} = 13\text{ Hz}$, $\text{Ru}-\text{CH}=\text{CH}$) and 8.22 (dt, $J_{\text{HH}} = 13\text{ Hz}$, $J_{\text{HP}} = 2\text{ Hz}$, $\text{Ru}-\text{CH}=\text{CH}$), the latter being additionally coupled to the two ^{31}P nuclei of the phosphine ligands. The *trans*-disposition of the phosphine ligands was evidenced by the observation of a singlet in the $^{31}\text{P}\{^1\text{H}\}$ NMR spectrum at $\delta\ 29.5\text{ ppm}$.

Reaction of red **2a** with excess PMe_3 gave the white complex $\text{Ru}\{\text{CH}=\text{CHC}_6\text{H}_4\text{N}(\text{C}_6\text{H}_4\text{Me}-4)_2-4\}\text{Cl}(\text{CO})(\text{PMe}_3)_3$ (**3a**) (Scheme 2), which is a further example of the *mer*- $\text{Ru}(\text{CH}=\text{CHR})\text{Cl}(\text{CO})(\text{PMe}_3)_3$ system [28, 46-48]. The vinyl proton resonances at 6.53 and 7.90 ppm displayed additional couplings to the three phosphine ligands, giving rise to a ddt pattern in each case, whilst in turn the

$^{31}\text{P}\{^1\text{H}\}$ NMR spectrum was characterised by a AM_2 pattern. The observation of the $\nu(\text{CO})$ band at 1919 cm^{-1} is consistent with the electronic trends of the supporting ligands. Further reaction of **2a-e** with the potassium salt of tris(pyrazolyl)borate (KTp) gave complexes $\text{Ru}(\text{CH}=\text{CHC}_6\text{H}_4\text{R-4})(\text{CO})(\text{PPh}_3)\text{Tp}$ (**4a-e**) bearing the *facially* capping Tp^- ligand [43, 49] (Scheme 2). With the exception of the orange-coloured NO_2 substituted derivative **4e**, these Tp complexes were isolated as pale yellow or green coloured solids. The choice of the Tp^- ligand was inspired by the analogy with the anionic cyclopentadienyl ligand that has been used to support many half-sandwich ruthenium complexes [50]. The Cp^- and Tp^- ligands are isoelectronic, six-electron donors, which usually coordinate in a tridentate manner, and lead to similar chemistry [51-54]. As KTp is a commercially available, air-stable solid, $[\text{Ru}(\text{CR}=\text{CHR})(\text{CO})(\text{PPh}_3)\text{Tp}]$ complexes are somewhat more readily available than the isoelectronic Cp analogues [43], and were chosen for studies of the electrochemical properties and electronic structure of ruthenium vinyl complexes.



Scheme 2. The preparation of **2a-e**, **3a** and **4a-e**.

The presence of the Tp^- ligand in the metal coordination sphere was readily apparent from the usual series of multiplets between 5.8 - 7.5 ppm arising from the pyrazoyl protons and the B-H resonance in the $^1\text{H}\{^{11}\text{B}\}$ spectrum at 4.64 ppm. In the ^{13}C NMR spectrum, the carbonyl carbon was observed as a doublet ($J_{\text{CP}} = 15 - 17$ Hz) near 207 ppm. The vinyl C_α carbon also gave rise to a characteristic doublet ($J_{\text{CP}} \sim 14$ Hz), the chemical shift of which was rather more sensitive to the nature of the vinyl substituent, and falling near δ 160 ppm for **4a**, **4b** and **4c** bearing the more electron-donating groups, and at 171.3 (**4d**) and 179.2 (**4e**) for those with strongly electron-withdrawing substituents, clearly demonstrating the effectiveness of conjugation through the vinyl ligand. The IR spectra of **4a-e** were characterised in each case by a $\nu(\text{CO})$ band which fell in the narrow range 1940 - 1946 cm^{-1} , whilst the $\nu(\text{B-H})$ band was observed between 2481 - 2485 cm^{-1} . The ^{31}P NMR spectra exhibited singlets between 49.4 - 51.3 ppm arising from the PPh_3 ligand. The complexes were further characterised by Atmospheric Solids Analysis Probe (ASAP) ionisation mass spectrometry [54], which gave clean spectra containing either the molecular ion, $[\text{M}]^+$, or the protonated form, $[\text{M}+\text{H}]^+$, and the structures confirmed by single crystal X-ray diffraction studies.

Reaction of $\text{RuHCl}(\text{CO})(\text{PPh}_3)_3$ with $\text{HC}\equiv\text{CC}_6\text{H}_4\text{CN-4}$ (**1f**) typically proceeds to give a yellow solution, likely containing a polymeric species $\{\text{Ru}(\text{CH}=\text{CHC}_6\text{H}_4\text{CN})(\text{CO})(\text{PPh}_3)_2\}_n$. Whilst we were unable to conclusively characterise this species, on one occasion addition of KTp gave small quantities of $\text{Ru}(\text{CH}=\text{CHC}_6\text{H}_4\text{CN-4})(\text{CO})(\text{PPh}_3)\text{Tp}$ (**4f**), which was identified crystallographically and found to be isostructural with **4c** and **4e**. In the absence of full spectroscopic

characterisation, and the capricious nature of the synthesis, the results of the structure determination have been included in the supporting information but no further study of this compound has been undertaken.

2.2 Molecular Structures

Single crystals of **3a** and **4b - e** were grown from CH₂Cl₂ / hexane (**3a**, **4b**, **4c**) or CH₂Cl₂ / MeOH (**4d**, **4e**). Plots of these molecules are shown in Figures 1 - 5, and Crystallographic data and important bond lengths and bond angles are summarised in the caption to Figure 1, and **Tables 1, 2** and **3**.

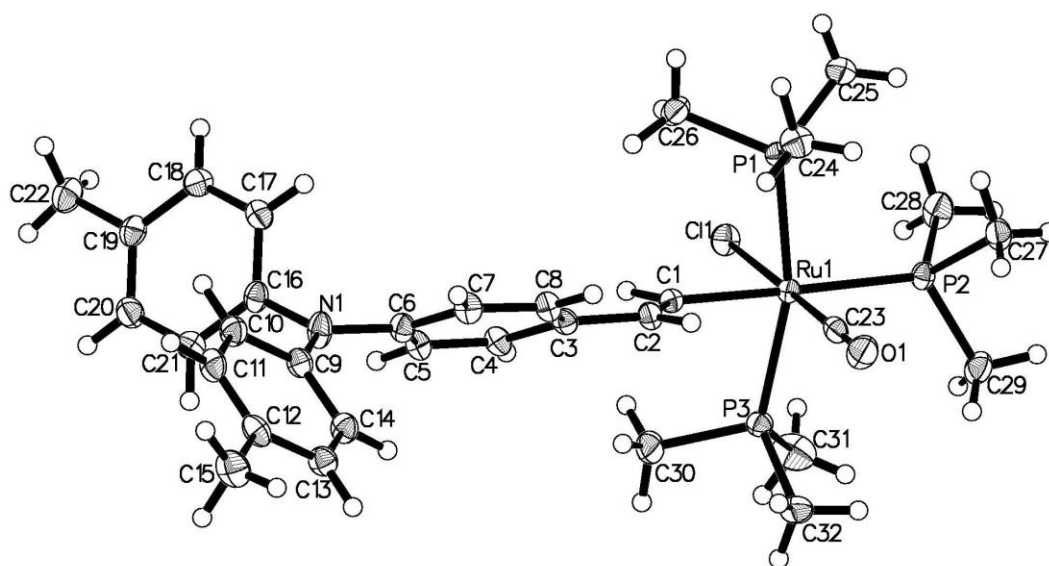


Figure 1. A plot of a molecule of **3a**, showing the atom-labeling scheme. Thermal ellipsoids in this and all subsequent figures are plotted at the 50 % probability level. Selected bond lengths (Å) and angles (°): Ru(1)-P(1) 2.3539(5); Ru(1)-P(2) 2.3919(4); Ru(1)-P(3) 2.3657(5); Ru(1)-Cl(1) 2.4617(5); Ru(1)-C(23) 1.8602(19); Ru(1)-C(1) 2.1165(15); C(1)-C(2) 1.339(2); C(2)-C(3) 1.480(2); N(1)-C(6) 1.422(2); N(1)-C(9) 1.408(2); N(1)-C(16) 1.433(2); P(1)-Ru(1)-P(2) 95.73(2); P(1)-Ru(1)-Cl(1)

86.11(2); P(1)-Ru(1)-C(23) 94.16(5); P(1)-Ru(1)-C(1) 82.37(4); P(1)-Ru(1)-P(3)
164.31(2).

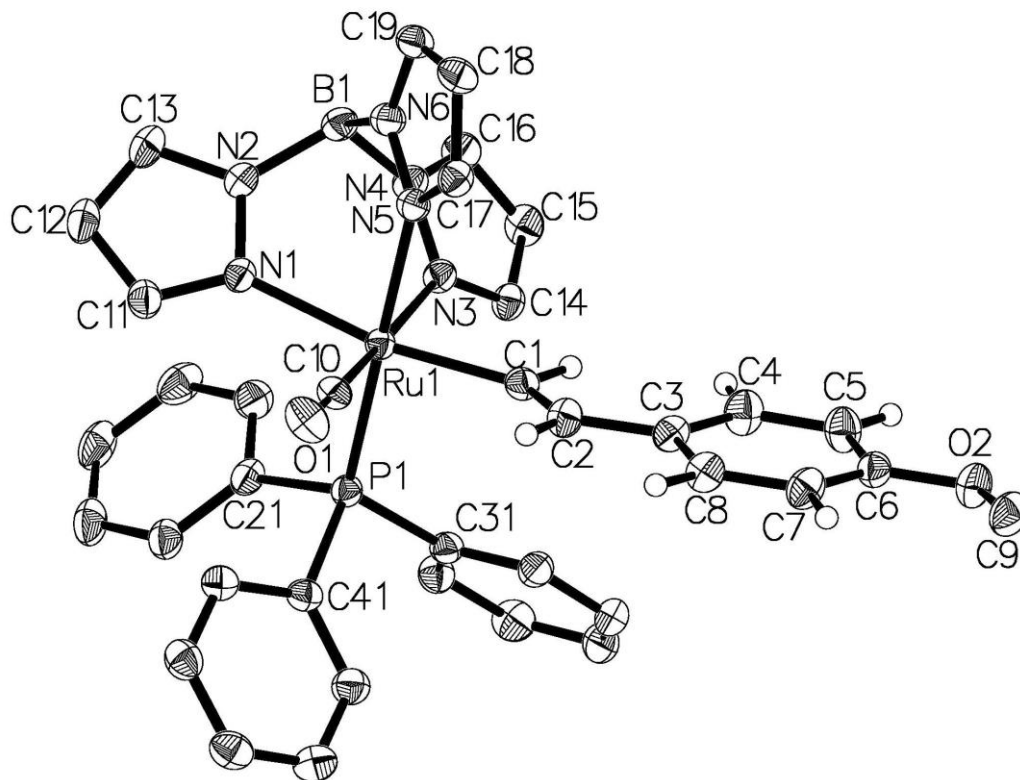


Figure 2. A plot of a molecule of **4b**, showing the atom-labeling scheme.

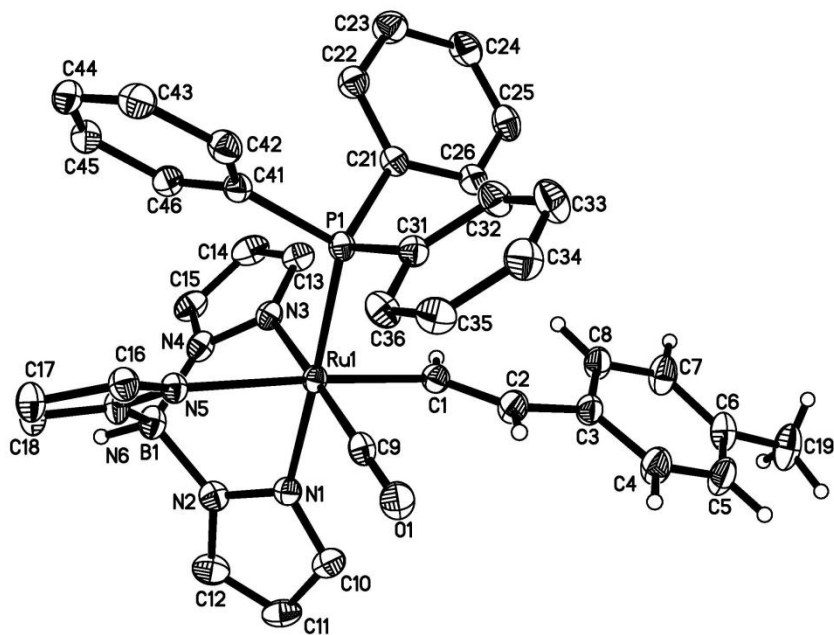


Figure 3. Plot of a molecule of **4c**, showing the atom-labeling scheme.

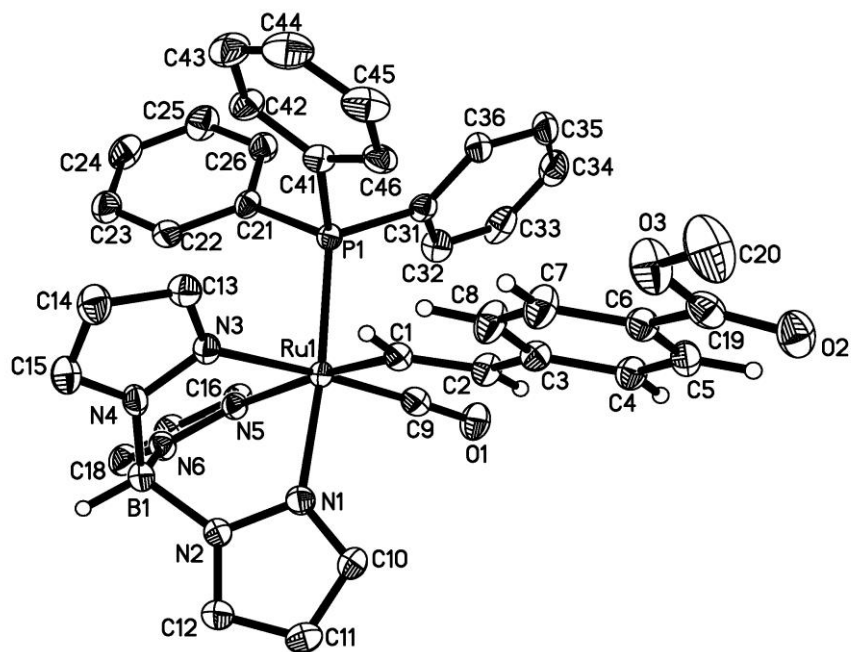


Figure 4. Plot of a molecule of **4d**, showing the atom-labeling scheme.

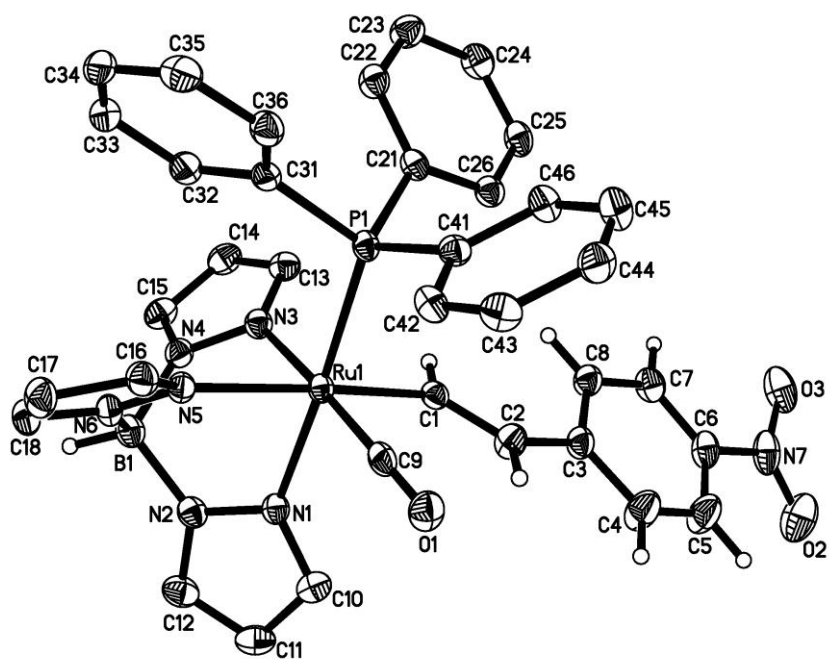


Figure 5. A plot of a molecule of **4e**, showing the atom-labeling scheme.

Table 1. Crystal Data and Structure Refinement for compounds **3a**, **4b-4f**

Complex	3a	4b	4c	4d	4e	4f
Empirical formula	C ₃₂ H ₄₇ ClNOP ₃ Ru	C ₃₇ H ₃₄ BN ₆ O ₂ PRu	C ₃₇ H ₃₄ BN ₆ OPRu	C ₃₉ H ₃₆ BCl ₂ N ₆ O ₃ PRu	C ₃₆ H ₃₁ BN ₇ O ₃ PRu	C ₃₇ H ₃₁ BN ₇ OPRu
Formula weight (g mol ⁻¹)	691.14	737.55	721.55	850.49	752.53	732.54
Crystal system	Triclinic	Orthorhombic	Monoclinic	Orthorhombic	Monoclinic	Monoclinic
Space group	P-1	Pbca	P 2 ₁ /n	Pca2 ₁	P2 ₁ /n	P2 ₁ /n
a (Å)	11.5356(3)	15.1780(3)	12.3553(4)	17.9655(9)	12.2388(2)	12.3271(4)
b (Å)	12.9757(4)	18.1705(3)	17.5258(6)	13.7346(7)	17.7482(3)	17.7540(5)
c (Å)	13.3499(4)	24.3305(5)	15.5575(5)	15.5579(9)	15.5664(3)	15.5549(4)
α (°)	64.04(1)	90.00	90.00	90.00	90.00	90
β (°)	70.43(1)	90.00	90.66(1)	90.00	90.36(10)	90.19(1)
γ (°)	78.61(1)	90.00	90.00	90.00	90.00	90.0
Volume (Å ³)	1689.77(8)	6710.2(2)	3368.54(19)	3838.9(4)	3381.21(10)	3404.3(2)
Z	2	8	4	4	4	4

ρ_{calc} Mg/m ³	1.358	1.460	1.423	1.472	1.478	1.429
μ , (mm ⁻¹)	0.710	0.559	0.553	0.635	0.559	0.549
F(000)	720	3024	1480	1736	1536	1496
Reflections collected	30109	98899	44956	30441	42882	38474
Independent reflections/ R_{int}	9862	8512/0.0626	9799/0.0607	10183/0.0273	8573/0.0727	8972/0.0898
Data / restraints / parameters	9862/0/540	8512/0/569	9799 / 0 / 560	10183/1/483	8573/0/450	8972/0/437
Goodness-of-fit on F^2	1.064	1.069	1.026	1.047	0.986	0.976
Final R_1 indices [$I > 2\sigma(I)$]	0.0286	0.0361	0.0324	0.0380	0.0334	0.0409
wR_2 indices (all data)	0.0344	0.0990	0.0820	0.1069	0.0847	0.0809

Table 2. Selected bond lengths for **4b - e**.

R	OMe	Me	CO ₂ Me	NO ₂
Complex	4b	4c	4d	4e
Ru(1)-C(1)	2.049(3)	2.0582 (19)	2.038 (3)	2.044 (2)
Ru(1)-P(1)	2.3249(6)	2.3193 (5)	2.3360 (8)	2.3315 (6)
Ru(1)-N(1)	2.125(2)	2.1407 (16)	2.121 (2)	2.1368 (19)
Ru(1)-N(3)	2.143(2)	2.1555 (16)	2.167 (3)	2.1504 (19)
Ru(1)-N(5)	2.190(2)	2.1952 (5)	2.179 (2)	2.1879 (18)
C(1)-C(2)	1.329(4)	1.342 (3)	1.352 (4)	1.338 (3)
C(2)-C(3)	1.470(4)	1.474 (3)	1.472 (4)	1.466 (3)
Ru(1)-C(9)	1.836(3)	1.8273 (19)	1.833 (3)	1.829 (2)
C(9)-O(1)	1.149(3)	1.153(2)	1.154(4)	1.154(3)

Table 3. Selected bond angles and dihedral angles for **4b - e**.

R	OMe	Me	CO ₂ Me	NO ₂
Complex	4b	4c	4d	4e
C(9)-Ru(1)-C(1)	91.03(11)	86.52 (8)	88.72 (12)	87.42 (10)
C(9)-Ru(1)-N(3)	174.77(9)	172.72 (7)	174.54 (12)	173.36 (9)
C(1)-Ru(1)-N(5)	169.78(9)	171.96 (7)	171.04 (10)	171.91 (8)
C(9)-Ru(1)-P(1)	92.61(8)	92.75 (6)	93.37 (10)	92.32 (8)
C(1)-Ru(1)-P(1)	94.11(7)	91.92 (5)	92.78 (8)	92.46 (6)
N(1)-Ru(1)-P(1)	175.47(6)	177.27 (4)	174.19 (7)	176.85 (5)
C(2)-C(1)-Ru(1)	134.0(2)	132.10 (15)	134.3 (2)	131.89 (19)
C(1)-C(2)-C(3)	127.0(3)	127.02 (19)	125.2 (3)	126.9 (2)
C(9)-Ru(1)-C(1)-C(2)	-8.53	-7.83	-5.52	7.89
Ru(1)-C(1)-C(2)-C(3)	-173.40	173.57	-176.29	176.61
C(1)-C(2)-C(3)-C(8)	1.0	19.6	-2.5	18.3

The metal center in **3a** exhibits a distorted octahedral geometry, consistent with previous examples [28, 46]. The vinyl ligand is co-planar with the CO moiety (C(23)-Ru(1)-C(1)-C(2) 9.7°, a feature common to the vinyl complexes described here and elsewhere, and commented upon in more detail below. The nitrogen center is essentially planar, with the sum of angles at N(1) 360°, confirming the sp² nature of this atom. The planes of vinyl and phenyl (C3-C8) groups are not parallel (torsion angle C1-C2-C3-C4 is 24.1°) and aromatic rings around N1 atom adopt the usual “propeller” configuration.

The compounds **4b - e** crystallize in centrosymmetrical space groups and therefore are racemic mixtures of two enantiomers. The Tp⁻ anion acts as a facial tridentate ligand occupying three coordination sites, and hence the ruthenium metal center exhibits a distorted octahedral geometry. Within the series **4b - e**, the Ru-C(9) [1.8273(19) – 1.833(3) Å], Ru-P [2.3193(5) – 2.3360(8) Å] and Ru-C(1) [2.038(3) – 2.0582(19) Å] bond lengths are comparable with those of related hydorruthenated compounds such as [Ru(CH=CHC₃H₇)Cl(CO)(PPh₃)₂(Me₂Hpz)] [Ru-CO; 1.79(1) Å, Ru-P; 2.319(3) Å, and Ru-C_α; 2.05(1) Å] [55] and [{RuCl(CO)(PPh₃)₂(Py)CH=CH}₃C₆H₃-1,3,5] [Ru-CO; 1.809(10) Å, Ru-P; 2.397(2) Å, and Ru-C_α; 2.050(8) Å] [56]. There is little or no evidence for significant quinoidal character within the phenylene portion of the molecule.

The strong *trans* influence of the σ -vinyl ligand noted above also causes an elongation of the Ru-N(5) distance. The vinyl ligand is essentially planar, with the C(1)-C(2)-C(3)-C(4)/C(8) torsion angle in the range 2.3 - 19.6°, although there are no obvious close inter-molecular contacts that might account for the variation between individual structures. The co-planar arrangement of the vinyl and carbonyl ligands has been noted previously [43], and arises to maximise back-bonding interactions between the metal d-orbitals with the vinyl and carbonyl π^* systems [57]. This preferential bonding situation that arises from a coplanar orientation of the carbonyl and vinyl ligands results in a significant energy barrier to rotation about the metal alkenyl bond, up to 10 kcal.mol⁻¹, which is significantly higher than values found in simple organic alkene molecules, where rotation is often less than 2 kcal.mol⁻¹ [58, 59]. Although a simple schematic MO description does not distinguish a preference for the vinyl ligand *cis* or *trans* to the CO ligand, detailed NBO analysis on related model systems suggests that the *cis* geometry is marginally (< 2 kcal.mol⁻¹) more stable [58]; steric effects may also play a role. It is also possible to speculate that intra-molecular C(2)-H... π (carbonyl) interactions may augment the preference of coplanar *cis*-orientation of vinyl and carbonyl ligands (the corresponding distances H...middle of CO are in range 2.49-2.82 Å).

2.3 Electrochemistry

Despite the close relationships between Tp⁻ and Cp⁻ [60], and the interest in the redox chemistry of both half-sandwich complexes bearing unsaturated ligands [20] and five and six-coordinate vinyl complexes [17], the redox chemistry of Ru(CH=CHC₆H₄R'-4)(CO)(PPh₃)Tp systems seems to have been barely explored. The six-coordinate Tp⁻

capped ruthenium vinyl complexes **4a** - **e** all show one or two (**4a**) oxidation waves at platinum working electrodes in CH₂Cl₂ / 0.1M NBu₄BF₄ at potentials that reflect the electronic properties of the aryl substituent (Table 4), but with some signs of slow electron transfer and chemical decomposition of the cations. Similar complications have been noted previously for Ru(CH=CHR)Cl(CO)(PMe₃)₃ derivatives [28]. Complex **4e** also has a reduction wave, reversible in CH₂Cl₂, which can be readily assigned to the reduction of the nitrophenyl moiety. The significant influence of the aryl ring substituent on the electrochemical potentials in the series of complexes **4a-e** indicates that the aryl group is likely closely associated with the redox-active orbitals. At a glassy carbon working electrode in NCMe / 0.1M NBu₄BF₄ the electrochemical response was fully electrochemically reversible at $\nu = 100$ mV / s, with linear dependence of peak current on $\nu^{1/2}$, peak-to-peak separation comparable with that of the internal ferrocene reference, and peak current ratios of unity. However, for consistency with the spectroelectrochemical experiments, which employ a cell with a Pt micromesh working electrode, voltammetric data from a Pt working electrode is reported here; potential variations between the Pt and C electrodes are negligible.

Table 4. Electrochemical data for **4a-e**.^a

Complex	R	E _{1/2} / V
4a^b	N(C ₆ H ₄ CH ₃) ₂	0.00
4b^c	OMe	0.14
4c	CH ₃	0.24
4d	CO ₂ Me	0.40
4e^d	NO ₂	0.51

^a Data acquired in 0.1 M NBu₄BF₄ in CH₂Cl₂ using a platinum working electrode, platinum counter and reference electrodes at a scan rate of 100 mV s⁻¹ and referenced to FcH/[FcH]⁺ = 0 V reported for comparison with spectroelectrochemical experiments conducted under similar conditions. ^b A reversible oxidation was observed at 0.39 V attributed to the oxidation of the amine moiety. ^c An irreversible oxidation was observed at E_{pa} 0.64 V attributed to the oxidation of the anisole moiety. ^d A reversible reduction was observed at -1.72 V for the nitro moiety.

2.4 IR Spectroelectrochemistry

The $\nu(\text{CO})$ and $\nu(\text{B-H})$ bands provide convenient tools through which to assess the structural and electronic changes that accompany the variation in redox state using spectroelectrochemical methods [61]. Metal-based oxidations usually result in a shift in $\nu(\text{C}\equiv\text{O})$ of $\sim +100 \text{ cm}^{-1}$, due to the substantial decrease in metal-carbonyl back-bonding [62]. On oxidation of the complexes **4a-e** there is a shift in $\nu(\text{C}\equiv\text{O})$ of *ca.* $+30 - 50 \text{ cm}^{-1}$ (Table 5), which compares with the *ca.* $+20 - 65 \text{ cm}^{-1}$ that results from the oxidation of closely related systems $[\text{Ru}(\text{CH}=\text{CHAr})\text{Cl}(\text{CO})(\text{P}^i\text{Pr}_3)_2(\text{L})]$ (Ar = Ph, pyrenyl; L = 4-ethyl-isonicotinate, vacant coordination site) and interpreted in terms of redox non-innocent vinyl ligands [18]. In the present examples, the concept of a substantial degree of ligand involvement in the redox process is supported by the small shift in the $\nu(\text{B-H})$ of $\sim +15 \text{ cm}^{-1}$, which indicates that the Tp⁻ ligand is hardly affected by the oxidation process. In addition, for **4d** the ester carbonyl also exhibited a small shift (*ca.* $+11 \text{ cm}^{-1}$, $\nu(\text{CO})$ 1708 to 1719 cm^{-1}) which compares with the $+3 - 5 \text{ cm}^{-1}$ shift in the isonicotinate ester bands upon oxidation of the five-coordinate complexes $[\text{Ru}(\text{CH}=\text{CHR}')\text{Cl}(\text{CO})(\text{P}^i\text{Pr}_3)_2(\text{py})]$ (R' = Bu^t, Ph, 1-pyrene, py = 4-ethyl-isonicotinate) in which the ester reporting group is connected via a pyridine ligand to the metal center [18]. Consistent with the voltammetric data in CH₂Cl₂, a degree of decomposition of the radical cations was evident in most complexes, with a persistent band at *ca.* 1973 cm^{-1} being formed with a concomitant decrease in the intensity of the parent spectrum on back-reduction. Attempts to probe the dication **[4a]²⁺** were compromised by rapid decomposition of the sample at the platinum mini-grid working electrode of the spectroelectrochemical cell.

Table 5. IR spectroelectrochemical data for **[4a - e]ⁿ⁺** (n = 0, 1) in 0.1 M NBu₄BF₄ in CH₂Cl₂, and calculated frequencies from **[4a' - e']ⁿ⁺** (n = 0, 1).^a

		Neutral		Cation			
	R	$\nu(\text{C}\equiv\text{O}) / \text{cm}^{-1}$	$\nu(\text{B-H}) / \text{cm}^{-1}$	$\nu(\text{C}\equiv\text{O}) / \text{cm}^{-1}$	$\nu(\text{B-H}) / \text{cm}^{-1}$	$\Delta\nu(\text{C}\equiv\text{O}) / \text{cm}^{-1}$	$\Delta\nu(\text{B-H}) / \text{cm}^{-1}$
4a	N(C ₆ H ₄ CH ₃) ₂	1940	2482	1973	2490	33	8
4a' ^b		1939	2550	1961	2573	22	23
4b	OMe	1940	2481	1992	2497	52	16
4b'		1938	2550	1974	2581	36	32
4c	CH ₃	1942	2484	1995	2496	53	12
4c'		1939	2551	1980	2583	42	33
4d^c	CO ₂ Me	1944	2482	1995	2496	51	14
4d'		1940	2552	1984	2446	45	34
4e	NO ₂	1946	2485	1996	2500	50	15
4e' ^d		1942	2555	1990	2589	49	35

^a a scaling factor of 0.98 applied to all calculated frequencies [63]

^b LS-[**4a'**]²⁺ $\nu(\text{CO})$ 1988; $\nu(\text{B-H})$ 2596 cm⁻¹; HS-[**4a'**]²⁺ $\nu(\text{CO})$ 1998; $\nu(\text{B-H})$ 2598 cm⁻¹

^c also $\nu(\text{CO}_{\text{ester}})$: **4d** 1708, [**4d**]⁺ 1719 cm⁻¹; [**4d'**] 1696; [**4d'**]⁺ 1698 cm⁻¹

^d [**4e'**]⁻ $\nu(\text{CO})$ 1927; $\nu(\text{B-H})$ 2531 cm⁻¹

2.5 Electronic structure calculations

The use of DFT based calculations in support of electrochemical and spectroscopic data to determine details of molecular electronic structure is now firmly established [6, 64], although correlation problems continue to provide challenges for the design of appropriate functionals [65, 66]. The computational models **4a'-e'** were constructed using the same ligands as in the real complexes with no symmetry constraints. The 'prime' nomenclature is used to distinguish the computational and experimental systems. We have found on previous occasions that B3LYP / 3-21G* generally gives computational results which are in good agreement with experimentally determined

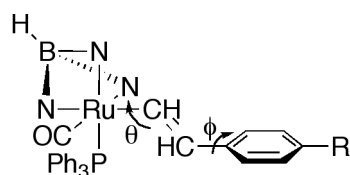
structural and spectroscopic properties for both ruthenium acetylide [20] and vinyl [28] complexes. However, in the case of $[\mathbf{4a}']^n$ ($n = 0, +1, +2$), $[\mathbf{4b}']^n$ ($n = 0, +1$), $[\mathbf{4c}']^n$ ($n = 0, +1$), $[\mathbf{4d}']^n$ ($n = 0, +1$) and $[\mathbf{4e}']^n$ ($n = -1, 0, +1$), it proved necessary to use the LANL2DZ basis set on Ru (3-21G* on all other atoms) to obtain optimised structures free of imaginary frequencies. There is very good agreement between the available crystallographically determined structures of **4b** - **4e** and the DFT optimised geometries, denoted **4a'** - **4e'** (Table 6), and also between spectroelectrochemically observed and calculated $\nu(\text{C}\equiv\text{O})$ and $\nu(\text{B-H})$ frequencies (Table 5), although the $\nu(\text{B-H})$ values were consistently over-estimated in the calculations.

Table 6 Selection of critical bond lengths from the crystallographically determined structures of **4b**, **4c**, **4d** and **4e**, and the corresponding bond lengths from the optimised geometries of the model systems $[\mathbf{4a}']^n$ ($n = 0, +1, +2$), $[\mathbf{4b}']^n$ ($n = 0, +1$), $[\mathbf{4c}']^n$ ($n = 0, +1$), $[\mathbf{4d}']^n$ ($n = 0, +1$) and $[\mathbf{4e}']^n$ ($n = -1, 0, +1$).

	Ru-C _{α}	C _{α} =C _{β}	C _{β} -C _{ipso}	Ru-P	Ru-N ₁ (<i>trans</i> phosphine)	Ru-N ₃ (<i>trans</i> CO)	Ru-N ₅ (<i>trans</i> vinyl)
4a'	2.0696	1.3513	1.4767	2.3742	2.1435	2.1814	2.2319
$[\mathbf{4a}']^+$	2.0090	1.3828	1.4361	2.4175	2.1490	2.1631	2.2142
LS- $[\mathbf{4a}']^{2+}$	1.9579	1.4180	1.4021	2.4564	2.1471	2.1470	2.1902
HS- $[\mathbf{4a}']^{2+}$	2.0526	1.3621	1.4694	2.4703	2.1431	2.1413	2.1642
4b	2.049(3)	1.329(4)	1.470(4)	2.3249(6)	2.125(2)	2.143(2)	2.190(2)
4b'	2.0717	1.3504	1.4786	2.3769	2.1423	2.1807	2.2338
$[\mathbf{4b}']^+$	1.9953	1.3871	1.4375	2.4377	2.1475	2.1577	2.2094
4c	2.0582(19)	1.342(3)	1.474(3)	2.3193(5)	2.1407(16)	2.1555(16)	2.1952(15)
4c'	2.0705	1.3505	1.4788	2.3773	2.1423	2.1799	2.2335
$[\mathbf{4c}']^+$	1.9944	1.3850	1.4439	2.4459	2.1540	2.1540	2.2068
4d	2.038(3)	1.352(4)	1.472(4)	2.3360(8)	2.121(2)	2.167(3)	2.179(2)
4d'	2.0655	1.3529	1.4736	2.3795	2.1428	2.1778	2.2312
$[\mathbf{4d}']^+$	1.9979	1.3824	1.4490	2.4526	2.1455	2.1488	2.2022
4e	2.044(2)	1.338(3)	1.466(3)	2.3315(6)	2.1368(19)	2.1504(19)	2.1879(18)

4e'	2.0601	1.3554	1.4686	2.3835	2.1432	2.1768	2.2277
[4e'] ⁺	2.0045	1.3775	1.4549	2.4597	2.1448	2.1474	2.1955
[4e'] ⁻	2.0718	1.3596	1.4620	2.3774	2.1422	2.1797	2.2566

The computed structures **4a'** - **e'** are remarkably consistent, with little variation in response to the electronic character of the vinyl ligand substituent despite the high degree of conjugation between the metal and aryl moiety suggested by the almost coplanar arrangement of the vinyl ligand, phenylene ring and substituent (torsion angles: $\theta = \text{CO-Ru-C}_\alpha\text{-C}_\beta$; $\phi = \text{C}_\alpha\text{-C}_\beta\text{-C}_{\text{ipso}}\text{-C}_{\text{ortho}}$, Figure 6). For example, the $\text{C}_\alpha\text{=C}_\beta$ bond lengths in **4a'** - **e'** fall between 1.3504 - 1.3554 Å, whilst the Ru-P bond length, which has been used as a relatively sensitive structural probe of electron density at the metal center [67], falls in the small range 2.1423 - 2.1435 Å. This structural invariance in the Ru-P bond length likely reflects the stronger back-bonding character of the vinyl π^* system which competes with the phosphine for electron-density from the same metal d-orbital. The computed and observed $\nu(\text{CO})$ frequencies also display little variation across the series **4a'** - **4e'** and together these structural and spectroscopic data suggest that there is little electronic influence of the ligand on the local electronic environment at the metal center.



	θ	ϕ
4a'	9.67	4.65
4b'	8.25	4.64
4c'	-10.16	-9.51
4d'	10.21	7.99
4e'	-7.78	-3.92

Figure 6. A schematic representation of the torsion angles ($^{\circ}$) θ and ϕ from the optimised geometries **4a'** - **e'**.

Table 7. Energy (eV) and composition (%) of selected frontier orbitals **4a'** - **e'**

		ϵ (eV)	%Tp	%PPh ₃	%CO	%Ru	%CH=CH	%Ar	%R
4a'	LUMO+9	+0.13	2	0	0	0	0	10	88
	LUMO+5	-0.19	55	21	15	7	1	1	0
	LUMO+4	-0.20	7	38	0	2	13	31	9
	LUMO+3	-0.39	11	64	4	6	5	8	2
	LUMO	-0.76	4	85	1	8	1	1	0
	HOMO	-4.31	1	1	0	9	17	25	47
	HOMO-1	-5.10	5	2	0	30	19	9	36
4b'	LUMO+10	+0.63	3	1	3	2	0	91	0
	LUMO+8	+0.38	21	12	5	6	18	36	2
	LUMO	-0.71	4	85	1	8	1	0	0
	HOMO	-4.47	3	2	0	22	33	33	8
4c'	LUMO+8	+0.28	32	15	1	4	13	33	1
	LUMO	-0.73	4	85	1	8	1	0	0
	HOMO	-4.64	4	2	0	28	35	30	1
4d'	LUMO+1	-0.80	5	63	1	9	3	13	7
	LUMO	-0.91	2	24	1	3	13	38	19
	HOMO	-4.92	5	2	0	33	34	24	3
4e'	LUMO+1	-0.98	5	82	2	10	1	0	0
	LUMO	-2.03	0	0	0	1	7	28	64
	HOMO	-5.21	6	2	0	37	32	20	3

In general, the HOMO is delocalised over the metal, vinyl moiety and substituent. However, in the case of **4a'** the HOMO is rather more heavily weighted on the triarylamine fragment, which is consistent with the low oxidation potentials of triarylamines [68], and it is the HOMO-1 which offers character similar to the HOMO in the other members of the series. Plots of the HOMO, LUMO and LUMO+1 for **4b'** which are representative of the key molecular orbitals across the series are given in Figure 7, whilst orbital energies and composition of selected important frontier orbitals are summarised in Table 7, with more complete lists given in the supporting information. In the neutral systems **4b'** - **e'**, the metallic contribution

to the HOMO and HOMO-1 is modestly sensitive to the nature of the substituent, with vinyl ligand contribution and HOMO energy greater for those systems bearing electron-donating substituents (**4b**, **4c**). Similarly significant contributions (67 – 84 %) of the vinyl ligand to the HOMOs in complexes $[\text{Ru}(\text{CH}=\text{CHAr})\text{Cl}(\text{CO})(\text{PMe}_3)_2]$ (Ar = Ph, Py) have been computed by Winter and his team [18]. Thus, in each case, the HOMO is predominately comprised of a Ru-CH=CH-Ar π -type system and can be termed a “metal-ligand” (ML) orbital (Figure 7, Table 7). The corresponding vinyl ligand π^* system features an appreciably smaller metal contribution (Figure 7, Table 7) and can be designated a “ligand” (L) orbital. The energy of this π^* orbital is also sensitive to the electronic nature of the aryl substituent, and comprises the LUMO for **4d'** and **4e'**, LUMO+4 for **4a'** and LUMO+8 for **4b'** and **4c'**. For **4a'**, **4b'** and **4c'** the LUMO is essentially a phosphine σ^* -orbital, with contributions from the metal center.

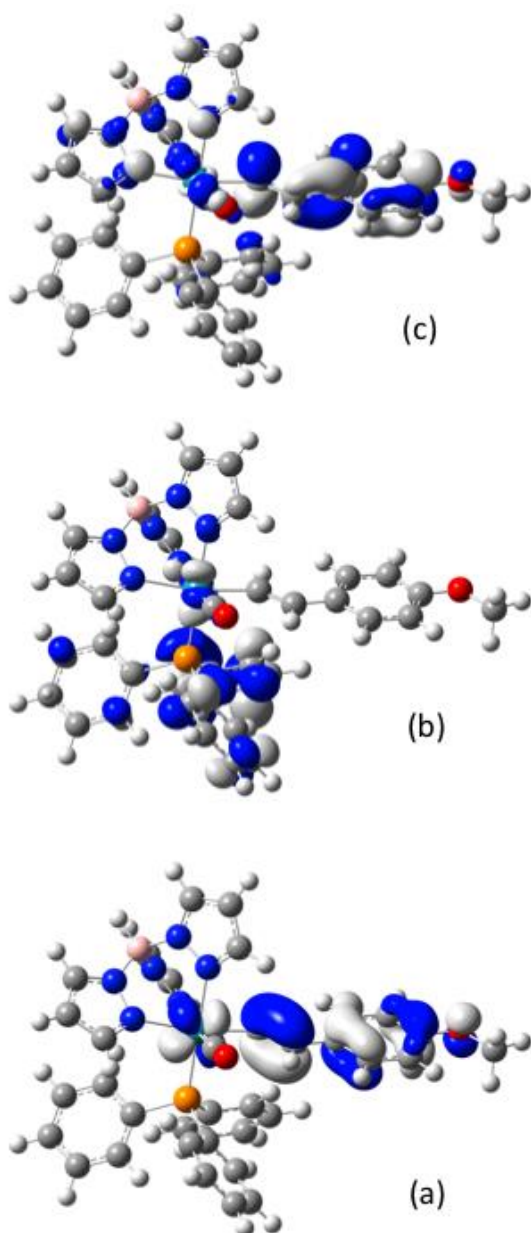


Figure 7. Plots of the HOMO, LUMO and LUMO+1 for **4b'**. In this and the subsequent figures, orbitals are plotted with contour values at ± 0.04 (e/bohr³)^{1/2}.

This description of the electronic structure is further supported by the UV-vis-NIR spectra of **4a** - **e**. The UV-vis-NIR spectrum of each complex **4a** - **e** is characterised by an intense absorption envelope which decreases in energy **4b** > **4a** > **4c** >> **4d** >> **4e** (Figure 8, Table 8) and assigned to the vinyl ligand π - π^* transition, which may perhaps be better described as $d\pi$ - π^* given the nature of the molecular orbitals. In addition, **4a** features a characteristic N(p)-Ar(π^*) transition envelope near 31850 cm⁻¹

[69]. These suggestions are in agreement with the results of TD DFT calculations, the results of which are summarised in Table 8.

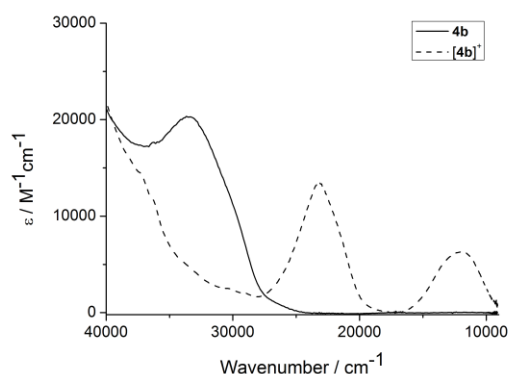


Figure 8. The UV-vis-NIR spectra of **4b** and **[4b]⁺** obtained by spectroelectrochemical methods (CH_2Cl_2 / 0.1 M NBu_4BF_4)

Table 8. Principal UV-vis absorption bands [$\nu_{\text{max}} / \text{cm}^{-1}$ ($\epsilon / \text{M}^{-1} \text{cm}^{-1}$)] observed from 0.1 M TBABF_4 in CH_2Cl_2 solutions of **[4a-e]ⁿ⁺** ($n = 0, 1$) and results of TD DFT calculations.

Complex	R	Wavenumber / cm^{-1} , [$\epsilon / \text{M}^{-1} \text{cm}^{-1}$]	TD DFT excitations / cm^{-1} (oscillator strength) and principal character
4a	$\text{N}(\text{C}_6\text{H}_4\text{CH}_3)_2$	31850 [27530],	31675 ($f = 0.2326$) HOMO \rightarrow LUMO+9
		29500 [32300]	29545 ($f = 0.3834$) HOMO \rightarrow LUMO+4

			28835 ($f = 0.2331$) HOMO \rightarrow LUMO+5 27609 ($f = 0.1860$) HOMO \rightarrow LUMO+3
[4a] ⁺		20530 [18250] 8640 [20350]	23580 ($f = 0.2276$) α -HOSO \rightarrow α -LUSO β -HOSO-17 \rightarrow β -LUSO 9875 ($f = 0.5151$) β -HOSO \rightarrow β -LUSO
4b	OMe	33560 [20270]	35644 ($f = 0.1791$) HOMO \rightarrow LUMO+8 HOMO \rightarrow LUMO+10
[4b] ⁺		23420 [13200] 12220 [6240]	27226 ($f = 0.4696$) α -HOSO \rightarrow α -LUSO β -HOSO-17 \rightarrow β -HOSO 13496 ($f = 0.1233$) β -HOSO-5 \rightarrow β -LUSO β -HOSO \rightarrow β -LUSO 11302($f = 0.1397$) β -HOSO \rightarrow β -LUSO
4c	CH ₃	32900 [18570]	36144($f = 0.2991$) HOMO \rightarrow LUMO+8
[4c] ⁺		24390 [3270] 13040 [1070]	27771 ($f = 0.3614$) α -HOSO \rightarrow α -LUSO β -HOSO-17 \rightarrow β -LUSO 13198 ($f = 0.1311$) β -HOSO \rightarrow β -LUSO
4d	CO ₂ Me	27930 [31960]	29606 ($f = 0.5414$) HOMO \rightarrow LUMO HOMO \rightarrow LUMO+1
[4d] ⁺		22320 [2190] 13120 [700]	25500 ($f = 0.0537$) α -HOSO \rightarrow α -LUSO β -HOSO-19 \rightarrow β -LUSO 12744 ($f = 0.1267$) β -HOSO \rightarrow β -LUSO
4e	NO ₂	22830 [28750]	23757 ($f = 0.4830$) HOMO \rightarrow LUMO
[4e] ⁺		16050 [4020] 12800 [1070]	14085 ($f = 0.0940$) β -HOSO-3 \rightarrow β -LUSO 12230 ($f = 0.0695$) β -HOSO \rightarrow β -LUSO β -HOSO-1 \rightarrow β -LUSO

The orbital characteristics described for the neutral systems are largely retained upon oxidation (Figure 9, Table 9), although the α -LUSO is essentially comprised of the vinyl ligand π^* system admixed with some metal character in each case, evidencing a degree of electronic and structural relaxation on oxidation. The β -HOSO is rather more metal in character (Table 9). In addition, the metallic contribution to the β -LUSO is generally somewhat greater than in the HOMO of the corresponding neutral system, although in the case of $[4a']^+$ there is a substantial contribution from the triarylamine moiety to this orbital and the amine group clearly is important in stabilising the charge in this rather delocalised system. The structural differences between the neutral complexes **4a'** - **e'** and the radical cations $[4a' - e']^+$ reflect the composition and nodal properties of the HOMO (Figure 7, Table 7) in **4a'** - **e'** and β -LUSO in $[4a' - e']^+$ (Figure 9, Table 9).

Table 9. Energy (eV) and composition (%) of selected spin orbitals $[4a' - 4e']^+$.

		ϵ (eV)	%Tp	%PPh ₃	%CO	%Ru	%CH=CH	%C ₆ H ₄	%R
[4a']⁺	α -LUSO	-3.45	2	3	1	4	29	50	12
	β -LUSO	-6.05	2	1	0	18	23	29	26
	α -HOSO	-7.35	3	1	0	13	19	29	36
	β -HOSO	-7.70	10	1	0	29	8	13	39
	β -HOSO-17	-9.59	45	11	1	7	5	10	21
[4b']⁺	α -LUSO	-3.70	2	7	1	5	39	42	4
	β -LUSO	-6.49	4	2	0	31	30	27	6
	α -HOSO	-8.08	4	2	0	16	26	40	12
	β -HOSO	-8.58	28	3	1	27	8	24	10
	β -HOSO-5	-9.29	22	37	3	28	3	5	3
	β -HOSO-17	-10.64	33	3	2	21	31	7	4
[4c']⁺	α -LUSO	-3.81	3	8	2	5	39	42	1
	β -LUSO	-6.65	5	2	0	37	30	24	1

	α -HOSO	-8.39	6	2	0	17	29	43	3
	β -HOSO	-8.84	35	5	1	22	11	24	2
	β -HOSO-17	-10.87	24	11	2	18	30	13	2
[4d] ⁺	α -LUSO	-4.19	2	2	1	4	31	48	12
	β -LUSO	-6.84	6	2	0	41	28	20	2
	α -HOSO	-8.64	7	2	0	17	30	39	4
	β -HOSO	-9.02	38	7	1	19	13	21	2
	β -HOSO-19	-11.01	22	14	2	17	28	14	3
[4e] ⁺	α -LUSO	-4.92	1	0	0	2	13	34	49
	β -LUSO	-7.13	8	2	0	46	25	16	3
	α -HOSO	-9.00	10	3	0	18	31	35	3
	β -HOSO	-9.28	46	9	1	19	11	12	1
	β -HOSO-1	-9.32	55	14	3	20	4	4	0
	β -HOSO-3	-9.50	12	74	1	6	3	4	0

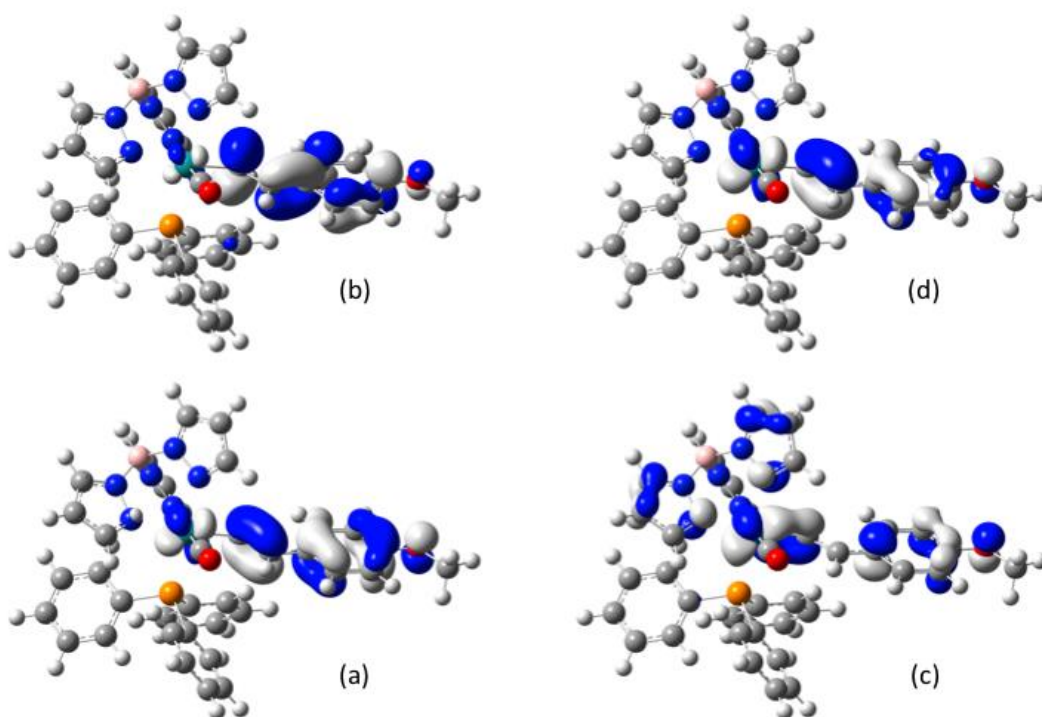


Figure 9. Plots of the (a) α -HOSO (b) α -LUSO (c) β -HOSO and (d) β -LUSO for [4d]⁺.

The calculated $\nu(\text{C}\equiv\text{O})$ frequencies are in good agreement with those observed from the spectroelectrochemical experiments, and the small increase in frequency of the $\nu(\text{C}\equiv\text{O})$ band upon oxidation is consistent with small metal contribution to the β -LUSO. Spin density calculations on the optimised geometries of $[\mathbf{4a}' - \mathbf{e}']^+$ support these general conclusions, with the vinyl ligand supporting progressively more of the electron spin as the donating properties of the vinyl substituent increase (Figure 10). As noted above regarding the composition of the β -LUSO, the spin density distribution in $[\mathbf{4a}']^+$ reinforces the concept that the triarylamine moiety plays an important role in stabilising the charge generated after oxidation.

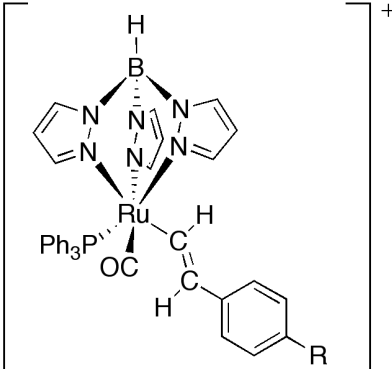
	Spin density				
	Ru	CH=CH	C ₆ H ₄	R	
	[4a']⁺	0.22	0.25	0.24	0.29 (N = 0.19)
	[4b]⁺	0.40	0.30	0.23	0.08
	[4c]⁺	0.48	0.30	0.22	0.00
	[4d]⁺	0.54	0.28	0.17	0.01
	[4e]⁺	0.61	0.24	0.12	0.01
	HS-[4a']²⁺	0.76	0.15	0.17	0.84 (N = 0.38)

Figure 10. A summary of the spin density distribution in $[\mathbf{4a}' - \mathbf{e}']^+$ and HS- $[\mathbf{4a}']^{2+}$

The computational methods also allow clarification of the nature of the electrochemically observed species $[\mathbf{4a}]^{2+}$ and $[\mathbf{4e}]^-$. The low-spin (singlet) dication $[\mathbf{4a}']^{2+}$, is calculated to lie some 0.16 eV lower in energy than the high-spin (triplet) state. The optimised geometries of LS- and HS- $[\mathbf{4a}']^{2+}$ (Table 6) are conveniently represented by the limiting valence bond descriptions given in Figure 11. These simple descriptions are supported further by the spin density distribution in the case of the open-shell system HS- $[\mathbf{4a}']^{2+}$ (Figure 10). Thus, whilst the HS state is well described in terms of localised Ru(III) and triarylamminium cations, the lower energy

LS state has a more delocalised electronic structure which would be more in keeping with the description of the redox product in terms of a doubly oxidised styrene, supported by the strongly electron-donating $\{\text{Ru}(\text{CO})(\text{PPh}_3)\text{Tp}\}$ and $\{\text{N}(\text{C}_6\text{H}_4\text{Me-4})_2\}$ moieties. There is little difference in the structures of $\mathbf{4e}'$ and $[\mathbf{4e}']^-$ (Table 6) and analysis of the LUMO composition of $\mathbf{4e}$ and spin density distribution in $[\mathbf{4e}']^-$ suggests that electrochemical reduction of can be described entirely satisfactorily in terms of a NO_2 based redox event.

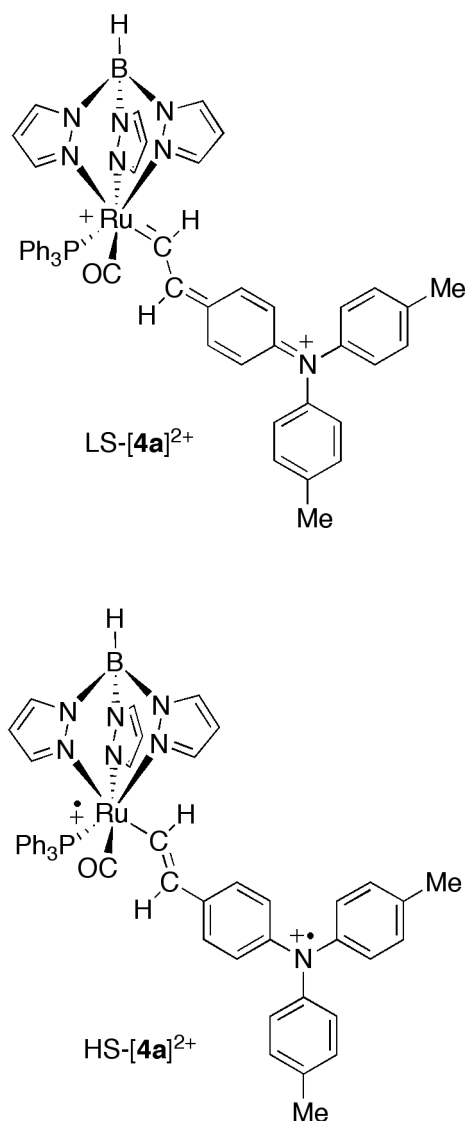


Figure 11. Valence bond descriptions of LS- and HS- $[\mathbf{4a}']^{2+}$.

In the UV-vis-NIR spectroelectrochemical studies, oxidation of $\mathbf{4b} - \mathbf{e}$ to $[\mathbf{4b} - \mathbf{e}]^+$ causes a shift of the $d\pi-\pi^*$ (or ML-LCT) transition to lower energy by 5000 - 10000

cm⁻¹, with a new transition in the NIR region near 10,000 cm⁻¹ (1160 - 760 nm) (Figure 8). These new, low energy bands can largely be assigned to excitations from the β -HOSO to the β -LUSO and therefore have more MLCT character. With the exception of [4e]⁺, the visible band corresponds to the α -HOSO to α -LUSO excitation, admixed with excitations involving a lower lying β -spin orbital and β -LUSO of similar composition (Table 8, Table 9). The absorption band therefore arises from excitations with essentially the same d π - π^* (ML-LCT) character as the UV band in the neutral species. For [4e]⁺, which carries the most electron withdrawing substituent, the visible band is much lower in energy, weak, and has much more significant MLCT character. In the case of oxidation of 4a to [4a]⁺ both ML-LCT and N(p)-Ar(π^*) transitions collapsed, reflecting the mixed metal / nitrogen character of the HOMO in 4a' and the α - and β -HOSO and LUSO in [4a']⁺.

3. Conclusions

The studies described above have shown that the vinyl ligand in the complexes [Ru(CH=CHC₆H₄R-4)(CO)(PPh₃)Tp]ⁿ⁺ (n = 0, 1) is significantly involved in both the HOMO of the neutral complexes and the β -LUSO of the monocations. Thus, the suspicions concerning the nature of redox products derived from five- and six-coordinate vinyl ligands raised by Winter are confirmed here for Tp⁻ supported complexes. The involvement of the vinyl ligand in the redox-active orbitals is reflected in the sensitivity of the oxidation potential E_{1/2} to the electronic character of the vinyl ligand substituent, and the relatively small positive shift of the ν (C≡O) frequencies that accompany oxidation of 4a - e, which is also reproduced in frequency calculations. UV-vis-NIR spectroelectrochemistry, spin density calculations and

analysis of the frontier molecular and spin orbitals are also consistent with this description in terms of a significant contribution of the vinyl ligand to the oxidation event. The relative contribution of metal atom and vinyl ligand to the frontier orbitals is sensitive to the vinyl ligand substituent, permitting a degree of tuning of the electronic structure.

4. Experimental

4.1 General conditions All reactions were carried out under an atmosphere of nitrogen, using standard Schlenk techniques. Reaction solvents were purified and dried using an Innovative Technology SPS-400, and degassed before use. No special precautions were taken to exclude air during the workup. The compounds $\text{RuHCl}(\text{CO})(\text{PPh}_3)_3$ [70], **1d** and **1e** [71] were prepared by literature methods. **1a** was prepared by desilylation of $\text{Me}_3\text{SiC}\equiv\text{CC}_6\text{H}_4\text{N}(\text{C}_6\text{H}_4\text{Me-4})_2$ [72]. Other reagents were purchased (Sigma-Aldrich) and used as received.

The NMR spectra were recorded on a 400 MHz Bruker Avance spectrometer from deuterated chloroform solutions and referenced against residual protio solvent resonances (CHCl_3 : ^1H 7.26 ppm; ^{13}C 77.0 ppm) or external phosphoric acid. In ^{13}C NMR assignments, the carbons on the aromatic ring are labelled C1 – C4 from the ethynyl substituent, and C5 – C8 for the tolyl ring carbons in **2a**, **3a** and **4a** from the N center. The carbons on the phosphine ligands are labelled C_i, C_o, C_m, C_p relative to the P center. IR spectra were recorded using a Thermo 6700 spectrometer from CH_2Cl_2 solutions in a cell fitted with CaF_2 windows. MALDI-mass spectra of organometallic complexes were recorded using Autoflex II TOF/TOF mass

spectrometer (Bruker Daltonik, GmbH) equipped with a 337 nm laser. Samples in CH_2Cl_2 (1 mg / ml) were mixed with a matrix solution of trans-2-[3-(4-tert-butylphenyl)-2-methyl-2-propenylidene]malononitrile (DCTB) in a 1:9 ratio, with 1 μl of mixture spotted onto a metal target prior to exposure to the MALDI ionization source. Accurate mass measurements were recorded with a *Xevo QToF* mass spectrometer (Waters Ltd, UK) equipped with an Agilent 7890 GC (Agilent Technologies UK Ltd, UK) Exact mass measurements utilised a lock-mass correction to provide < 3 mDa precision†. Exact mass measurement used Elemental Composition version 4.0 embedded within MassLynx 4.1 (Waters Ltd, UK).

Electrochemical analyses were carried out using an EcoChemie Autolab PG-STAT 30 potentiostat, with platinum working, platinum counter and platinum pseudo reference electrodes, from solutions in CH_2Cl_2 containing 0.1 NBu_4BF_4 , $v = 100 - 800 \text{ mV s}^{-1}$. All redox potentials are reported with reference to an internal standard of the ferrocene/ferrocenium couple ($\text{FcH}/\text{FcH}^+ = 0.0 \text{ V}$) [73]. Spectroelectrochemical measurements were made in an OTTLE cell of Hartl design [74], from CH_2Cl_2 solutions containing 0.1 M NBu_4BF_4 electrolyte. The cell was fitted into the sample compartment of the Nicolet Avatar, Thermo 6700, Thermo Array UV-Vis or Perkin-Elmer Lambda 900 spectrophotometer and electrolysis in the cell was performed with a PGSTAT-30 potentiostat.

The single-crystal X-ray data were collected at 120.0(2)K on a Bruker SMART-CCD 1K (compound **4f**) and Bruker SMART CCD 6000 (all other compounds) diffractometers ($\lambda\text{Mo-K}\alpha$, $\lambda = 0.71073 \text{ \AA}$, ω -scan, $0.3^\circ/\text{frame}$) equipped with Cryostream (OxfordCryosystems) open-flow nitrogen cryostat. The data for **4b-4e**

were corrected for absorption using SADABS (**4b** and **4d**) and face-indexed numerical absorption correction procedures. The structures were solved by direct method and refined by full-matrix least squares on F^2 for all data using SHELXTL [75] and OLEX2 [76] software. All non-hydrogen atoms were refined with anisotropic displacement parameters, H-atoms were located on the difference map and refined isotropically in structures **3a**, **4b** and **4c**, while in the rest of the structures the hydrogen atoms were placed in calculated positions and refined in riding mode. The crystallographic and refinement parameters are given in the supporting information.

4.2 Syntheses

4.2.1 Preparation of $(CH_3C_6H_4)_2N(C_6H_4CH=CHRu(CO)Cl(PPh_3)_2)$ (**2a**)

To a suspension of $RuHCl(CO)(PPh_3)_3$ (0.20 g, 0.210 mmol) in dry CH_2Cl_2 (8 ml) was added $(CH_3C_6H_4)_2N(C_6H_4C\equiv CH)$ (0.08 g, 0.250 mmol). The reaction was stirred for 40 minutes after which the solvent was removed. Addition of hexane (6 ml) to the red residue dissolved in CH_2Cl_2 (1 ml) led to the formation of a pink powder. A red powder was produced from CH_2Cl_2 (2 ml) and methanol (10 ml) and dried under vacuum (0.16 g, 79 %). Precipitation by CH_2Cl_2 and diethylether gave the analytically pure sample (67 mg, 22 %). 1H NMR: δ 2.30 (s, 6H, CH_3), 5.54 (d, $^3J_{HH} = 13$ Hz, $RuCH=CH$), 6.62 (d, $^3J_{HH} = 8$ Hz, Ar), 6.80 (d, $^3J_{HH} = 8$ Hz, Ar), 6.96 (d, $^3J_{HH} = 8$ Hz, 4H, Ar- CH_3), 7.04 (d, $^3J_{HH} = 8$ Hz, 4H, Ar- CH_3), 7.35 – 7.58 (m, 30H, PPh_3), 8.22 (dt, $^3J_{HH} = 13$ and $^4J_{HP} = 2$ Hz, 1H, $RuCH=CH$). ^{13}C NMR: δ 20.9 (s, CH_3), 123.2 ($C_{2/3}$), 124.3 ($C_{6/7}$), 125.2 ($C_{2/3}$), 128.5 (t, $^3J_{CP} = 5$ Hz, $C_{m/m'}$), 129.9 ($C_{6/7}$), 130.3 (s, $C_{p/p'}$), 132.0 (d, $^1J_{CP} = 16$ Hz, $C_{i/i'}$), 132.2 (s, C_8), 133.4 (s, C_4), 134.4 (t, $^2J_{CP} = 5$ Hz, $C_{o/o'}$), 135.4 (t, $^4J_{CP} = 3$ Hz, Ru_β), 144.2 (t, $^3J_{CP} = 12$ Hz, Ru_α), 144.9 (s, C_1), 145.7 (s, C_5), 201.8 (unresolved, CO). ^{31}P NMR: δ 29.5. IR (CH_2Cl_2): $\nu(CO)$ 1932 cm^{-1} . MALDI(+)-MS: 987.2 $[M]^+$.

4.2.2 Preparation of $(CH_3C_6H_4)_2N(C_6H_4CH=CHRu(CO)Cl(PMe_3)_3)$ (**3a**)

To a suspension of $RuHCl(CO)(PPh_3)_3$ (0.10 g, 0.105 mmol) in dry CH_2Cl_2 was added $(CH_3C_6H_4)_2N(C_6H_4C\equiv CH)$ (0.03 g, 0.105 mmol). The reaction was stirred for 30 minutes and then PMe_3 was added (0.07 ml, 0.630 mmol) and the reaction stirred for a further 12 hours. The solvent was removed *via* Schlenk techniques and the resultant oil triturated with hexane to produce a light yellow powder. Purification by preparative TLC using hexane and acetone (70:30) produced a white powder (0.05 g, 67 %). Crystallisation from CH_2Cl_2 layered with hexane by slow diffusion gave crystals suitable for X-ray diffraction. 1H NMR: δ 1.40 (t, $^4J_{HH} = 4$ Hz, 18H, PMe_3), 1.47 (d, $^4J_{HH} = 8$ Hz, 9H, PMe_3), 2.29 (s, 6H, CH_3), 6.47 – 6.53 (unresolved ddt, 1H $RuCH=CH$), 6.93 (d, $^3J_{CP} = 8$ Hz, 2H, Ar), 6.98 (d, $^3J_{CP} = 8$ Hz, 4H, Ar), 7.03 (d, $^3J_{CP} = 8$ Hz, 4H, Ar), 7.17 (d, $^3J_{CP} = 8$ Hz, 2H, Ar), 7.87 – 7.94 (ddt, $^3J_{HH} = 20$ Hz, $^3J_{H-P(trans)} = 8$ Hz, $^3J_{HP} = 4$ Hz, 1H, $RuCH=CH$). ^{13}C NMR: δ 17.0 (td, $^1J_{CP} = 15$ and $^3J_{CP} = 3$ Hz, PMe_3), 20.5 (dt, $^1J_{CP} = 20$ Hz $^3J_{CP} = 3$ Hz, PMe_3), 21.1 (s, CH_3), 124.1 (s, $C_{6/7}$), 124.2 (s, $C_{2/3}$), 125.3 (s, $C_{2/3}$), 130.0 (s, $C_{6/7}$), 131.8 (s, C_8), 134.6 (t, $^3J_{CP} = 4$ Hz, C_β), 136.8 (dt, $^4J_{CP(trans)} = 8$ and $^4J_{CP} = 3$ Hz, C_1), 144.7 (s, C_4), 146.1 (s, C_5), 163.3 (dt, $^2J_{CP(trans)} = 77$ Hz, $^2J_{CP} = 18$ Hz, C_α), 202.8 (q, $^2J_{CP} = 12$ Hz, CO). ^{31}P NMR: δ -6.82 (d, $J = 23$ Hz, PMe_3), -18.63 (t, $J = 23$ Hz, PMe_3). IR (CH_2Cl_2): $\nu(CO)$ 1919 cm^{-1} . MALDI(+)-MS: 615.1 $[M-PMe_3]^+$, 587.1 $[M-PMe_3-CO]^+$.

4.2.3 Preparation of $[Ru(CO)(PPh_3)Tp](CH=CHC_6H_4N(C_6H_4CH_3)_2)$ (**4a**)

To a suspension of $RuHCl(CO)(PPh_3)_3$ (0.30 g, 0.315 mmol) in dry CH_2Cl_2 (10 ml) was added $(CH_3C_6H_4)_2N(C_6H_4C\equiv CH)$ (0.11 g, 0.377 mmol). The reaction was

allowed to stir for 30 minutes and then KTp (0.16 g, 0.631 mmol) was added. After 18 hours, the yellow green solution was filtered through Celite, and the solvent removed. The residue was redissolved in the minimum amount of CH₂Cl₂ (1 ml) and methanol (8 ml) was added to produce a yellow precipitate. Purification by preparative TLC using CH₂Cl₂ and hexane (35:65) gave a light yellow powder (0.60 g, 21 %). ¹H NMR: δ 2.31 (s, 6H, CH₃), 5.92 (t, ³J_{HH} = 2 Hz, Tp), 5.91 (t, ³J_{HH} = 2 Hz, Tp), 6.09 (unresolved t, 1H, Tp), 6.36 (d, 1H, ³J_{HH} = 16 Hz, RuCH=CH), 6.80 (dd, ³J_{HH} = 8 and ⁴J_{HP} = 4 Hz, 2H, 2 x Tp), 6.94 (d, ³J_{HH} = 8 Hz, 2H, Ar), 6.99 (m, 10H, 2H Ar and 8H Ar'), 7.10 – 7.15 (m, 6H, PPh₃), 7.21 – 7.26 (m, 6H, PPh₃), 7.34 – 7.38 (m, 3H, PPh₃), 7.58 (unresolved triplet, 1H, Tp), 7.70 (dd, ³J_{HH} = 17 and ⁴J_{HP} = 2 Hz, 2H, 2 x Tp), 7.34 (m, 1H, Tp), 8.08 (dd, ³J_{HH} = 16 and ³J_{HP} = 4 Hz, 1H, RuCH=CH). ¹³C NMR: δ 21.1 (s, CH₃), 105.2 (d, J = 2 Hz, Tp), 105.3 (s, Tp), 105.3 (s, Tp), 123.7 (s, C_{6/7}), 124.5 (s, C_{2/3}), 125.1 (s, C_{2/3}), 128.0 (d, ³J_{CP} = 9 Hz, C_{m/m'}), 129.7 (s, C_{6/7}), 129.8 (d, ⁴J_{CP} = 3 Hz, C_{p/p'}), 131.4 (s, C₈), 133.1 (d, ¹J_{CP} = 44 Hz, C_{i/i'}), 134.2 (d, ²J_{CP} = 9 Hz, C_{o/o'}), 134.5 (d, J = 3 Hz, Tp), 135.0 (s, Tp), 135.3 (s, Tp), 136.2 (s, C_β), 137.0 (s, C₁), 142.8 (s, Tp), 142.9 (s, Tp), 144.0 (s, Tp), 144.1 (s, C₄), 146.1 (s, C₅), 160.5 (d, ²J_{CP} = 12 Hz, C_α), 206.9 (d, ²J_{CP} = 17 Hz, CO). ³¹P NMR: δ 49.4. IR (CH₂Cl₂): ν(CO) 1940, ν(BH) 2482 cm⁻¹. MALDI(+)-MS: 903.2 [M]⁺. HR ASAP MS (*m/z*): 897.2664 C₅₀H₄₆BN₇OPRu requires 897.2707.

4.2.4 Preparation of [{Ru(CO)(PPh₃)(Tp)}(CH=CHC₆H₄OMe-*p*)] (**4b**)

To a suspension of RuHCl(CO)(PPh₃)₃ (0.100 g, 0.105 mmol) in CH₂Cl₂ (6 ml) was added 1-ethynyl-4-methoxybenzene (0.07 ml, 0.524 mmol). The solution turned red and was stirred for 30 min. KTp (0.080 g, 0.315 mmol) was added and the solution

turned green over the course of an hour. The solution was then filtered through Celite and the solvent removed. The residual solid was re-dissolved in CH₂Cl₂ (2 ml), hexane was added (4 ml) and some solvent removed. A light green powder was collected by filtration and dried under vacuum (0.036 g, 43 %). Crystals suitable for X-ray diffraction were obtained from the slow diffusion of hexane into a solution of CH₂Cl₂. ¹H NMR: δ 3.78 (s, 3H, OCH₃), 5.89 (t, ³J_{HH} = 2 Hz, 1H, Tp), 5.91 (t, ³J_{HH} = 2 Hz, 1H, Tp), 6.05 (unresolved t, 1H, Tp), 6.31 (d, ³J_{HH} = 17 Hz, 1H, Ru-CH=CH), 6.78 – 6.80 (m, 4H, 2H Tp and 2H C₆H₄), 7.08 – 7.14 (m, 8H, 6H PPh₃ and 2H C₆H₄), 7.20 – 7.23 (m, 6H, PPh₃), 7.33 – 7.36 (m, 3H, PPh₃), 7.56 (unresolved triplet, 1H, Tp), 7.68 – 7.71 (m, 3H, 3 x Tp), 7.97 (dd, ³J_{HH} = 17 Hz and ³J_{HP} = 4 Hz, 1H, RuCH=CH). ¹³C NMR: δ 55.7 (s, OMe), 105.4 (d, J = 3 Hz, Tp), 105.5 (s, 2 x Tp), 113.9 (s, C₃), 125.5 (s, C₂), 128.2 (d, ³J_{CP} = 9 Hz, C_{m/m'}), 130.0 (d, ⁴J_{CP} = 2 Hz, C_{p/p'}), 133.4 (d, ¹J_{CP} = 42 Hz, C_{i/i'}), 134.4 (d, ²J_{CP} = 10 Hz, C_{o/o'}), 134.7 (d, J = 2 Hz, Tp), 135.2 (s, Tp), 135.5 (s, Tp), 135.8 (s, C_β), 136.1 (s, C₁), 143.0 (s, Tp), 143.1 (s, Tp), 144.3 (s, Tp), 156.8 (s, C₄), 158.4 (d, ²J_{CP} = 14 Hz, C_α), 207.1 (d, ²J_{CP} = 17 Hz, CO). ³¹P NMR: δ 51.3. MALDI(+)-MS 738.2 [M + H]⁺. IR (CH₂Cl₂): ν(C≡O) 1940, ν(B-H) 2479 cm⁻¹. HR ASAP MS (*m/z*): 732.1760 [M + H]⁺ C₃₇H₃₅BN₆O₂PRu requires 732.1764.

4.2.5 Preparation of [{Ru(CO)(PPh₃)Tp}(CH=CHC₆H₄Me-*p*)] (**4c**)

The synthesis and workup is similar to **2**, with 1-ethynyl-4-methoxybenzene replaced by *p*-tolylacetylene. A pale yellow powder was collected by filtration and dried under vacuum (0.051 g, 64 %). Crystals suitable for X-ray diffraction were obtained from the slow diffusion of hexane into a CH₂Cl₂ solution. ¹H NMR: δ 2.30 (s, 3H, CH₃),

5.90 (t, $^3J_{\text{HH}} = 2$ Hz, 1H, Tp), 5.92 (t, $^3J_{\text{HH}} = 2$ Hz, 1H, Tp), 6.05 (t, $^3J_{\text{HH}} = 2$ Hz, 1H, Tp), 6.36 (d, $^3J_{\text{HH}} = 17$ Hz, 1H, Ru-CH=CH), 6.78 (dd, $^3J_{\text{HH}} = 12$ and $^3J_{\text{HP}} = 2$ Hz, 2H, 2 x Tp), 7.01 – 7.13 (m, 10H, 6H PPh₃, 4H C₆H₄), 7.19 – 7.24 (m, 6H, PPh₃), 7.33 – 7.37 (m, 3H, PPh₃), 7.55 (unresolved t, 1H, Tp), 7.67 – 7.70 (m, 3H, 3 x Tp), 8.14 (dd, $^3J_{\text{HH}} = 17$ Hz and $^3J_{\text{HP}} = 4$ Hz, 1H, RuCH=CH). ¹³C NMR: δ 21.3 (s, CH₃), 105.0 (d, $J = 3$ Hz, Tp), 105.1 (s, 2 x Tp), 124.3 (s, C₂), 127.9 (d, $^2J_{\text{CP}} = 9$ Hz, C_{m/m'}), 128.7 (s, C₃), 129.6 (d, $^4J_{\text{CP}} = 2$ Hz, C_{p/p'}), 132.9 (s, C₄), 133.0 (d, $^1J_{\text{CP}} = 42$ Hz, C_{i/i'}), 134.0 (d, $^3J_{\text{CP}} = 9$ Hz, C_{o/o'}), 134.4 (d, $J = 3$ Hz, Tp), 134.8 (s, Tp), 135.1 (s, Tp), 136.5 (s, C _{β}), 139.1 (s, C₁), 142.6 (s, Tp), 142.7 (s, Tp), 143.9 (s, Tp), 160.0 (d, $^2J_{\text{CP}} = 14$ Hz, C _{α}), 206.7 (d, $^2J_{\text{CP}} = 15$ Hz, CO). ³¹P NMR: δ 50.6. MALDI(+)-MS (m/z): 722.2 [M + H]⁺. IR (CH₂Cl₂): $\nu(\text{C}\equiv\text{O})$ 1942, $\nu(\text{B-H})$ 2481 cm⁻¹. HR ASAP MS (m/z) 715.1735 [M] C₃₇H₃₄BN₆OPRu requires 715.1737.

4.2.6 Preparation of [*Ru(CO)(PPh₃)Tp*](CH=CHC₆H₄CO₂Me-*p*)] (**4d**)

The synthesis and workup is similar to **2**, with 1-ethynyl-4-methoxybenzene replaced by methyl 4-ethynylbenzoate. A light green powder was produced (0.134 g, 56 %). Crystals suitable for X-ray diffraction were obtained from the slow diffusion of methanol into a CH₂Cl₂ solution. ¹H NMR: δ 3.88 (s, 3H, OCH₃), 5.91 (t, $^3J_{\text{HH}} = 2$ Hz, 1H, Tp), 5.94 (t, $^3J_{\text{HH}} = 2$ Hz, 1H, Tp), 6.07 (unresolved t, 1H, Tp), 6.48 (d, $^3J_{\text{HH}} = 17$ Hz, 1H, RuCH=CH), 6.80 (dd, $^3J_{\text{HH}} = 8$ Hz and $^3J_{\text{HP}} = 2$ Hz, 2H, 2 x Tp), 7.04 – 7.09 (m, 6H, PPh₃), 7.13 (d, $J = 8$ Hz, 2H, C₆H₄), 7.18 – 7.23 (m, 6H, PPh₃), 7.31 – 7.35 (m, 3H, PPh₃), 7.52 (unresolved t, 1H, Tp), 7.60 (d, $^3J_{\text{HH}} = 2$ Hz, 1H, Tp), 7.71 (d.o.d, $^3J_{\text{HH}} = 8$ Hz and $^3J_{\text{HP}} = 2$ Hz, 2H, 2 x Tp), 7.87 (d, $^3J_{\text{HH}} = 8$ Hz, 2H, C₆H₄), 8.68 (dd, $^3J_{\text{HH}} = 17$ Hz and $^3J_{\text{HP}} = 4$ Hz, 1H, RuCH=CH). ¹³C NMR: δ 52.0 (s, OMe),

105.5 (d, $J = 2$ Hz, Tp), 105.6 (s, Tp), 105.7 (s, Tp), 124.2 (s, C₂), 125.0 (s, C₄), 128.3 (d, $^2J_{CP} = 10$ Hz, C_{m/m'}), 130.1 (s, C₃), 130.2 (d, $^4J_{CP} = 2$ Hz, C_{p/p'}), 133.0 (d, $^1J_{CP} = 43$ Hz, C_{i/i'}), 134.3 (d, $^3J_{CP} = 10$ Hz, C_{o/o'}), 134.9 (d, $J = 2$ Hz, Tp), 135.3 (s, Tp), 135.6 (s, Tp), 136.7 (s, C_β), 142.9 (s, Tp), 143.0 (s, Tp), 144.3 (s, Tp), 145.5 (s, C₁), 168.0 (s, CO of ligand), 171.3 (d, $^2J_{CP} = 13$ Hz, C_α), 206.8 (d, $^2J_{CP} = 16$ Hz, CO). ^{31}P NMR: δ 50.9. MALDI(+)-MS (m/z): 766.2 $[\text{M} + \text{H}]^+$. IR (CH₂Cl₂): $\nu(\text{C}\equiv\text{O})$ 1940, $\nu(\text{B-H})$ 2483 cm⁻¹. HR ASAP MS (m/z): 760.1742 $[\text{M} + \text{H}]^+$ C₃₈H₃₄BN₆O₃PRu requires 760.1714.

4.2.7 Preparation of [*Ru(CO)(PPh₃)Tp*](CH=CHC₆H₄NO₂-*p*)] (**4e**)

The synthesis and workup is similar to **2**, with 1-ethynyl-4-methoxybenzene replaced by 1-ethynyl-4-nitrobenzene. An orange powder was produced (0.152 g, 64 %). Crystals suitable for X-ray diffraction were obtained from the slow diffusion of methanol into a CH₂Cl₂ solution. ^1H NMR: δ 5.93 (t, $^3J_{HH} = 2$ Hz, 1H, Tp), 5.96 (t, $^3J_{HH} = 2$ Hz, 1H, Tp), 6.08 (unresolved t, 1H, Tp), 6.54 (d, $^3J_{HH} = 17$ Hz, 1H, Ru-CH=CH), 6.81 (dd, $^3J_{HH} = 16$ Hz and $^3J_{HP} = 2$ Hz, 2H, 2 x Tp), 7.03 – 7.07 (m, 6H, PPh₃), 7.13 (d, $^3J_{HH} = 9$ Hz, 2H, C₆H₄), 7.19 – 7.24 (m, 6H, PPh₃), 7.34 – 7.38 (m, 3H, PPh₃), 7.59 (unresolved m, 2H, Tp), 7.72 (dd, $^3J_{HH} = 12$ Hz and $^3J_{HP} = 2$ Hz, 2H, 2 x Tp), 8.06 (d, $^3J_{HH} = 12$ Hz, 2H, C₆H₄), 9.04 (dd, $^3J_{HH} = 17$ Hz and $^3J_{HP} = 4$ Hz, 1H, RuCH=CH). ^{13}C NMR: δ 105.6 (d, $J = 3$ Hz, Tp), 105.7 (s, Tp), 105.8 (s, Tp), 124.3 (s, C₂), 124.5 (s, C₃), 128.4 (d, $^2J_{CP} = 10$ Hz, C_{m/m'}), 130.0 (d, $^4J_{CP} = 2$ Hz, C_{p/p'}), 132.7 (d, $^1J_{CP} = 44$ Hz, C_{i/i'}), 134.2 (d, $^3J_{CP} = 10$ Hz, C_{o/o'}), 135.1 (d, $^3J_{CP} = 2$ Hz, Tp), 135.5 (s, Tp), 135.7 (s, Tp), 136.0 (s, C_β), 142.9 (d, $J = 3$ Hz, Tp), 144.0 (s, Tp), 144.4 (s, Tp), 146.6 (s, C₁), 179.2 (d, $^2J_{CP} = 12$ Hz, C_α), 206.5 (d, $^2J_{CP} = 16$ Hz, CO). *C₁ not

observed. ^{31}P NMR: δ 50.7. MALDI(+)-MS 753.10 $[\text{M} + \text{H}]^+$. IR (CH_2Cl_2): $\nu(\text{C}\equiv\text{O})$ 1945, $\nu(\text{B-H})$ 2485 cm^{-1} . HR ASAP MS (m/z): 747.1533 $[\text{M} + \text{H}]^+$ $\text{C}_{36}\text{H}_{32}\text{BN}_7\text{O}_3\text{PRu}$ requires 747.1510.

4.3 Computations All optimisations were carried out with the Gaussian 09 package [77] using the B3LYP [78] hybrid functional and the pseudopotential LANL2DZ [79] for Ru and the 3-21G* basis set [80] for all other atoms. These geometries were found to be true minima based on no imaginary frequencies found. Electronic structure and TD-DFT calculations were also carried out on the optimized geometries at the B3LYP/LANL2DZ:3-21G* level of theory. The MO diagrams and orbital contributions were generated with the aid of GaussView 5.0 [81] and GaussSum [82] packages, respectively.

Acknowledgements Financial support from the EPSRC is gratefully acknowledged. PJJ held a Research School of Chemistry Visiting Fellowship whilst on leave at the Australian National University, and holds an EPSRC Leadership Fellowship. JDF held a Durham University Doctoral Fellowship. WYM holds a studentship from the Durham Doctoral Training Account.

Appendix A. Supplementary material. Tables of energy (eV) and composition (%) of selected frontier orbitals. Crystallographic data for compounds **3a**, **4b**, **4c**, **4d**, **4e** and **4f** are deposited as CCDC 892268 - 892273. The data can be obtained free of charge from the Cambridge Crystallographic Data Centre via www.ccdc.cam.ac.uk/data_request/cif.

References

1. W. Kaim, *Inorg. Chem.* 50 (2011) 9752.
2. C.R. Jorgensen, *Coord. Chem. Rev.* 1 (1966) 164.
3. C.C. Scarborough, K. Wieghardt, *Inorg. Chem.* 50 (2011) 9773.
4. M.D Ward, J.A. McCleverty, *J. Chem. Soc., Dalton Trans.* (2002) 275.
5. F. Pevny, R.F. Winter, B. Sarkar, S. Zalis, *Dalton Trans.* 39 (2010) 8000.
6. S. Zalis, R.F. Winter, W. Kaim, *Coord. Chem. Rev.* 254 (2010) 1383.
7. W.I. Dzik, J.I. va der Vlugt, J.N.H. Reek, B. de Bruin, *Angew. Chem. Int. Ed.* 50 (2011) 3356.
8. A.L. Smith, K.I. Hardcastle, J.D. Soper, *J. Am. Chem. Soc.* 132 (2010) 14358.
9. P.J. Chirik, K. Wiegardt, *Science* 327 (2010) 794.
10. F.A. Cotton, G. Wilkinson, *Advanced Inorganic Chemistry*, pp 768, 4th Ed, 1980, John Wiley and Sons Inc., New York.
11. C.C. Scarborough, S. Sproules, T. Weyhermueller, S. DeBeer, K. Wieghardt, *Inorg. Chem.* 50 (2011) 12446.
12. B. Albinsson, M.P. Eng, K. Pettersson, M.U. Winters, *Phys. Chem. Chem. Phys.* 9 (2007) 5847.
13. M.I. Bruce, A. Burgun, F. Gendron, G. Grelaud, J.-F. Halet, B.W. Skelton, *Organometallics* 30 (2011) 2861.
14. F. Paul, B.G. Ellis, M.I. Bruce, L. Toupet, T. Roisnel, K. Costuas, J.-F. Halet, C. Lapinte, *Organometallics* 25 (2006) 649.
15. M.A. Fox, J.D. Farmer, R.L. Roberts, M.G. Humphrey, P.J. Low, *Organometallics* 28 (2009) 5266.

16. N. Gauthier, N. Tchouar, F. Justaud, G. Argouarch, M.P. Cifuentes, L. Toupet, D. Touchard, J.-F. Halet, S. Rigaut, M.G. Humphrey, K. Costuas, F. Paul, *Organometallics* 28 (2009) 2253.
17. P. Muecke, M. Linseis, S. Zalis, R.F. Winter, *Inorg. Chim. Acta* 374 (2011) 36.
18. J. Maurer, M. Linseis, B. Sarkar, B. Schwederski, M. Niemeyer, W. Kaim, S. Zalis, C. Anson, M. Zabel, R.F. Winter, *J. Am. Chem. Soc.* 130 (2008) 259.
19. W.M. Khairul, M.A. Fox, P.A. Schauer, D. Albesa-Jove, D.S. Yufit, J.A.K. Howard, P.J. Low, *Inorg. Chim. Acta* 374 (2011) 461.
20. M.A. Fox, R.L. Roberts, W.M. Khairul, F. Hartl, P.J. Low, *J. Organomet. Chem.* 692 (2007) 3277.
21. J. Maurer, B. Sarkar, B. Schwederski, W. Kaim, R.F. Winter, S. Zális, *Organometallics* 25 (2006) 3701.
22. E. Wuttke, F. Pevny, Y.-M. Hervault, L. Norel, M. Drescher, R.F. Winter, S. Rigaut, *Inorg. Chem.* 51 (2012) 1902.
23. F. Pevny, E. Di Piazza, L. Norel, M. Drescher, R.F. Winter, S. Rigaut, *Organometallics* 29 (2010) 5912.
24. K. Costuas, S. Rigaut, *Dalton Trans.* 40 (2011) 5643.
25. A. Klein, O. Lavastre, J. Fiedler, *Organometallics* 25 (2006) 635.
26. D.J. Armit, M.I. Bruce, M. Gaudio, N.N. Zaitseva, B.W. Skelton, A.H. White, B. Le Guennic, J.-F. Halet, M.A. Fox, R.L. Roberts, F. Hartl, P.J. Low, *Dalton Trans.* (2008) 6763.
27. M.A. Fox, B. Le Guennic, R.L. Roberts, D.A. Brue, D.S. Yufit, J.A.K. Howard, G. Manca, J.-F. Halet, F. Hartl, P.J. Low, *J. Am. Chem. Soc.* 133 (2011) 1843.

28. W.Y. Man, J.-L. Xia, N.J. Brown, J.D. Farmer, D.S. Yufit, J.A.K. Howard, S.H. Liu, P.J. Low, *Organometallics* 30 (2011) 1852.
29. A.F. Hill, in: D.E. Shriver, M.I. Bruce (Eds.), *Comprehensive Organometallic Chemistry II*, vol. 7, Pergamon, Oxford, 1995, pp. 399–411.
30. H. Werner, M.A. Esteruelas, H. Otto, *Organometallics* 5 (1986) 2295.
31. H. Werner, U. Meyer, K. Peters, H.G. von Schnering, *Chem. Ber.* 122 (1989) 2089.
32. M.R. Torres, A. Vegas, A. Santos, J. Ros, *J. Organomet. Chem.* 309 (1986) 169.
33. M.R. Torres, A. Santos, J. Ros, X. Solans, *Organometallics* 6 (1987) 1091.
34. M.R. Torres, A. Vegas, A. Santos, J. Ros, *Organometallics* 7 (1988) 1233.
35. M.R. Torres, A. Vegas, A. Santos, J. Ros, *J. Organomet. Chem.* 326 (1987) 413.
36. S.K. Seetharaman, M.-C. Chung, U. Englich, K. Ruhlandt-Senge, M.B. Sponsler, *Inorg. Chem.* 46 (2007) 561.
37. A.F. Hill, R.P. Melling, *J. Organomet. Chem.* 396 (1990) C22.
38. S. Bohle, G.R. Clarke, C.E.F. Rickard, W.R. Roper, W.E.B. Shepard, L.J. Wright, *J. Chem. Soc. Chem. Commun.* (1987) 563.
39. A. Gieren, C. Ruizperez, T. Hubner, M. Herberhold, A.F. Hill, *J. Chem. Soc. Dalton Trans.* (1988) 1693.
40. W.R. Roper, G.E. Taylor, J.M. Waters, L.J. Wright, *J. Organomet. Chem.* 157 (1978) C27.
41. W.R. Roper, G.E. Taylor, J.M. Waters, L.J. Wright, *J. Organomet. Chem.* 182 (1979) C46.
42. M. Herberhold, A.F. Hill, *J. Organomet. Chem.* 395 (1990) 315.

43. N.W. Alcock, A.F. Hill, R.P. Melling, *Organometallics* 10 (1991) 3898.
44. J.D.E.T Wilton-Ely, S.J. Honarkhah, M. Wang, D.A. Tocher, A.M.Z. Slawin, *Dalton Trans.* (2005) 1930.
45. P. Muecke, M. Zabel, R. Edge, D. Collison, S. Clement, S. Zalis, R.F. Winter, *J. Organomet. Chem.* 696 (2011) 3186.
46. X. Wu, T. Weng, S. Jin, J. Liang, R. Guo, G.-a. Yu, S.H. Liu, *J. Organomet. Chem.* 694 (2009) 1877.
47. S.H. Liu, Q.Y. Hu, P. Xue, T.B. Wen, I.D. Williams, G. Jia, *Organometallics* 24 (2005) 769.
48. Y. Lin, J. Yuan, M. Hu, J. Cheng, J. Yin, S. Jin, S.H. Liu, *Organometallics* 28 (2009) 6402.
49. S.-H. Liu, H. Xia, K.L. Lok, R.C.Y. Yeung, Q.Y. Hu, G. Jia, *J. Organomet. Chem.* 683 (2003) 331.
50. J. Gimeno, V. Cadierno, in *Comprehensive Organometallic Chemistry III*, Chapter 6.15 pp 551 - 646, R.H. Crabtree, D.M.P. Mingos (Eds) Elsevier, Oxford.
51. M.A.J. Tenorio, M.J. Tenorio, M.C. Puerta, P. Valerga, *Organometallics* 16 (1997) 5528.
52. M.J. Tenorio, M.A.J. Tenorio, M.C. Puerta, P. Valerga, *Inorg. Chim. Acta.* 259 (1997) 77.
53. A.M. McNair, D.C. Boyd, K.R. Mann, *Organometallics* 5 (1986) 303.
54. C.N. McEwen, R.G. McKay, B.S. Larsen, *Anal. Chem.* 77 (2005) 7826.
55. M.R. Torres, A. Santos, A. Perales, J. Ros, *J. Organomet. Chem.* 353 (1988) 221.

56. H.P. Xia, T.B. Wen, Q. Y. Hu, X. Wang, X.G. Chen, L.Y. Shek, I.D. Williams, K.S. Wong, G.K.L. Wong, G.C. Jia, *Organometallics* 24 (2005) 562.
57. S.H. Choi, I. Bytheway, Z.Y. Lin, G.C. Jia, *Organometallics* 17 (1998) 3974.
58. K.B. Wiberg, E. Martin, *J. Am. Chem. Soc.* 107 (1985) 5035.
59. A.E. Dorigo, D.W. Pratt, K.N. Houk, *J. Am. Chem. Soc.* 109 (1987) 6591.
60. S.J. Trofimenko, *Prog. Inorg. Chem.* 34 (1986) 115.
61. S.P. Best, S.J. Borg, K.A. Vincent, in *Spectroelectrochemistry*, W. Kaim, A. Klein (Eds), Royal Society of Chemistry, Cambridge, 2008.
62. J. Maurer, R. F. Winter, B. Sarkar, J. Fieldler, S. Zalis, *Chem. Commun.* (2004) 1900.
63. (a) A.P. Scott, L. Radom, *J. Phys. Chem.* 100 (1996) 16502; (b) J.C. Roder, F. Meyer, I. Hyla-Kryspin, R.F. Winter, E. Kaifer, *Chem. Eur. J.* 9 (2003) 2636.
64. A. Vleck, S. Zalis, *Coord. Chem. Rev.* 251 (2007) 258.
65. A.V. Arbuznikov, M. Kaupp, *J. Chem. Phys.* 136 (2012) 014111.
66. J. Plotner, D.J. Tozer, A. Dreuw, *J. Chem. Theory Comput.* 6 (2010) 2315.
67. R.L. Cordiner, D. Albesa-Jové, R.L. Roberts, J.D. Farmer, H. Puschmann, D. Corcoran, A.E. Goeta, J.A.K. Howard, P.J. Low, *J. Organomet. Chem.* 690 (2005) 4908.
68. (a) P.J. Low, M.A.J. Paterson, A.E. Goeta, D.S. Yufit, J.A.K. Howard, J.C. Cherryman, D.R. Tackley, B. Brown, *J. Mater. Chem.* 14 (2004) 2516; (b) P.J. Low, M.A.J. Paterson, D.S. Yufit, J.A.K. Howard, J.C. Cherryman, D.R. Tackley, R. Brook, B. Brown, *J. Mater. Chem.* 15 (2005) 2304.

69. P.J. Low, M.A.J. Paterson, H. Puschmann, A.R. Goeta, J.A.K. Howard, C. Lambert, J.C. Cherryman, D.R. Tackley, S. Leeming, B. Brown, *Chem. Eur. J.* 10 (2004) 83.
70. N. Ahmad, J.J. Levison, S.D. Robinson, M.F. Uttley, *Inorg. Synth.* 15 (1974) 45.
71. O. Lavastre, L. Olivier, P. Dixneuf, *Tetrahedron* 15 (1996) 5495.
72. W.Y. Man, K.B. Vincent, H.J. Spencer, D.S. Yufit, J.A.K. Howard, P.J. Low, *J. Cluster Sci.* 2012 doi 10.1007/s10876-012-0482-y.
73. N.G. Connelly, W.E. Geiger, *Chem. Rev.* 96 (1996) 877.
74. M. Krejci, M. Danek, F. Hartl, *J. Electroanal. Chem.* 317 (1991) 179.
75. G.M. Sheldrick, *Acta Cryst. A* 64 (2008) 112.
76. O.V. Dolomanov, L.J. Bourhis, R.J. Gildea, J.A.K. Howard, H. Puschmann, *J. Appl. Cryst.* 42 (2009) 339.
77. Gaussian 09, Revision A.02, M. J. Frisch, G. W. Trucks, H. B. Schlegel, G. E. Scuseria, M. A. Robb, J. R. Cheeseman, G. Scalmani, V. Barone, B. Mennucci, G. A. Petersson, H. Nakatsuji, M. Caricato, X. Li, H. P. Hratchian, A. F. Izmaylov, J. Bloino, G. Zheng, J. L. Sonnenberg, M. Hada, M. Ehara, K. Toyota, R. Fukuda, J. Hasegawa, M. Ishida, T. Nakajima, Y. Honda, O. Kitao, H. Nakai, T. Vreven, J. A. Montgomery, Jr., J. E. Peralta, F. Ogliaro, M. Bearpark, J. J. Heyd, E. Brothers, K. N. Kudin, V. N. Staroverov, R. Kobayashi, J. Normand, K. Raghavachari, A. Rendell, J. C. Burant, S. S. Iyengar, J. Tomasi, M. Cossi, N. Rega, J. M. Millam, M. Klene, J. E. Knox, J. B. Cross, V. Bakken, C. Adamo, J. Jaramillo, R. Gomperts, R. E. Stratmann, O. Yazyev, A. J. Austin, R. Cammi, C. Pomelli, J. W. Ochterski, R. L. Martin, K. Morokuma, V. G. Zakrzewski, G. A. Voth, P. Salvador, J. J.

- Dannenberg, S. Dapprich, A. D. Daniels, O. Farkas, J. B. Foresman, J. V. Ortiz, J. Cioslowski, D. J. Fox, *Gaussian, Inc.*, Wallingford CT, 2009.
78. (a) A. D. Becke, *J. Chem. Phys.* 98 (1993) 5648; (b) C. Lee, W. Yang, R. G. Parr, *Phys. Rev. B* 37 (1988) 785.
79. (a) T. H. Dunning, Jr., P. J. Hay, in *Modern Theoretical Chemistry*, Editor: Schaefer, H. F. III, Vol. 3, Plenum, New York (1976) 1-28; (b) P. J. Hay, W. R. Wadt, *J. Chem. Phys.* 82 (1985) 270; (c) W. R. Wadt, P. J. Hay, *J. Chem. Phys.* 82 (1985) 284; (d) P. J. Hay, W. R. Wadt, *J. Chem. Phys.* 82 (1985) 299.
80. (a) G. A. Petersson, M. A. Al-Laham, *J. Chem. Phys.* 94 (1991) 6081; (b) G. A. Petersson, A. Bennett, T. G. Tensfeldt, M. A. Al-Laham, W. A. Shirley, J. Mantzaris, *J. Chem. Phys.* 89 (1988) 2193.
81. R.D. Dennington II, T.A. Keith, J.M. Millam, Gaussian Inc, Wallingford, CT, 2008.
82. N. M. O'Boyle, A. L. Tenderholt, K. M. Langner, *J. Comput. Chem.* 29 (2008) 839.